AWARD NUMBER: W81XWH-12-1-0374

TITLE: Platform for Rapid Delivery of Biologics and Drugs to Ocular Cells and Tissues Following Combat Associated Trauma

PRINCIPAL INVESTIGATOR: Rajendra Kumar-Singh, PhD

CONTRACTING ORGANIZATION: Trustees of Tufts College Inc.
Boston, MA 02111

REPORT DATE: September 2016

TYPE OF REPORT: Annual

PREPARED FOR: U.S. Army Medical Research and Materiel Command
Fort Detrick, Maryland 21702-5012

REPORT DOCUMENTATION PAGE

Form Approved
OMB No. 0704-0188

1. REPORT DATE	2. REPORT TYPE	3. DATES COVERED
September 2016	Annual	30 Aug 2015 - 29 Aug 2016

4. TITLE AND SUBTITLE
Platform for Rapid Delivery of Biologics and Drugs to Ocular Cells and Tissues Following Combat Associated Trauma

5a. CONTRACT NUMBER

5b. GRANT NUMBER
W81XWH-12-1-0374

5c. PROGRAM ELEMENT NUMBER

6. AUTHOR(S)

Rajendra Kumar-Singh, PhD

5d. PROJECT NUMBER

5e. TASK NUMBER

5f. WORK UNIT NUMBER

7. PERFORMING ORGANIZATION NAME(S) AND ADDRESS(ES)

Trustees of Tufts College Inc.
Boston, MA 02111

8. PERFORMING ORGANIZATION REPORT NUMBER

9. SPONSORING / MONITORING AGENCY NAME(S) AND ADDRESS(ES)
U.S. Army Medical Research and Materiel Command
Fort Detrick, Maryland 21702-5012

10. SPONSOR/MONITOR'S ACRONYM(S)

11. SPONSOR/MONITOR'S REPORT NUMBER(S)

12. DISTRIBUTION / AVAILABILITY STATEMENT
Approved for Public Release; Distribution Unlimited

13. SUPPLEMENTARY NOTES

14. ABSTRACT

The goals of this study are to develop a platform technology for protein delivery into retinal cells. We have published two manuscripts detailing successful completion of three of our four major goals.

15. SUBJECT TERMS-

16. SECURITY CLASSIFICATION OF:			17. LIMITATION OF ABSTRACT	18. NUMBER OF PAGES	19a. NAME OF RESPONSIBLE PERSON
a. REPORT	b. ABSTRACT	c. THIS PAGE			USAMRMC
U	U	U	UU	28	19b. TELEPHONE NUMBER *(include area code)*

Table of Contents

1. INTRODUCTION

The goal of this research is to develop a platform technology for the delivery of therapeutic proteins into retinal cells. Blast trauma to the eye leads to the initiation of cellular degenerative processes that lead to the death of a variety of cell types in the retina including the photoreceptors and ganglion cells. Death of these cells leads to blindness. These cellular processes include apoptosis, otherwise known as programmed cell death. Although there are many known inhibitors of apoptosis, there is currently no method available to deliver these inhibitors into retinal cells in vivo. The plasma membrane of cells acts as a barrier for the delivery of proteins into retinal cells. We envisage that in the combat theater, following blast trauma, the impacted member of the armed forces or a colleague utilizes the procedure of intravitreal injection to deliver an inhibitor of apoptosis to the retina as a way to attenuate the progression of apopotosis and ensuring cell death that is associated with blindness. In the civilian population, intravitreal injection is a standard office procedure performed on millions of Americans and thus we believe our approach to alleviate cell death in the combat theater is practical if we can overcome the delivery of macromolecules across the plasma membrane of retinal cells.

2. KEYWORDS

Apoptosis, blast trauma, Peptide for Ocular Delivery (POD), AS1411, Cell Penetrating Peptide, Protein Delivery, Photoreceptors, Ganglion Cells, Nucleolin

3. ACCOMPLISHMENTS

The major goals of this project are to develop:

a) Synthesize proteins that can cross the plasma membrane of cells when attached to a platform plasma permeating technology
b) Characterize the kinetics of these proteins in vitro
c) Characterize the kinetics of these proteins in vivo in retina and cornea
d) Demonstrate efficacy of these proteins in a model of uv light-induced apoptosis

To date we have completed the first three of the four primary goals. Details of our results for the first three goals are in the following publication attached to this report as an appendix:

G-quartet oligonucleotide mediated delivery of proteins into photoreceptors and retinal pigment epithelium via intravitreal injection.

Leaderer D, Cashman SM, Kumar-Singh R.

Experimental Eye Research. 2016 Apr;145:380-92. doi: 10.1016/j.exer.2016.02.009. Epub 2016 Feb 27.

We have found that the above technology is capable of inhibiting laser induced damage to the retina that leads to choroidal neovascularization (also a model of age related macular degeneration). This observation is published in the following manuscript:

Topical application of a G-Quartet aptamer targeting nucleolin attenuates choroidal neovascularization in a model of age-related macular degeneration.
Leaderer D, Cashman SM, Kumar-Singh R.

Exp Eye Res. 2015 Nov;140:171-8. doi: 10.1016/j.exer.2015.09.005. Epub 2015 Sep 12.

A summary of our progress on the fourth goal is as follows:

Detection of recombinant human XIAP by Western Blotting:
We generated various complexes of XIAP and biotin/AS1411. XIAP antibody was utilized to probe recombinant human XIAP (rhXIAP) in the complexes of biotinylated AS1411 and Traptavidin. Lane 1 - standard protein ladder. Lane 2 - recombinant XIAP. Lane 3 - biotinylated XIAP. Lane 4 - biotinylated XIAP - Traptavidin complex, the antibody could not access XIAP, hence the expected band is not observed. Lane 5 - biotinylated XIAP - Traptavidin - biotinylated AS1411 complex. Lane 6 - trypsin treatment of Lane 5

components. Lane 7 - complex treated with DNAse I. It is possible in both cases, enzymes could not access substrates because of steric hindrance. Lane 8 -is complex which contains non-biotinylated XIAP. Because of this complex formation is lacking, and antibody can recognize XIAP.

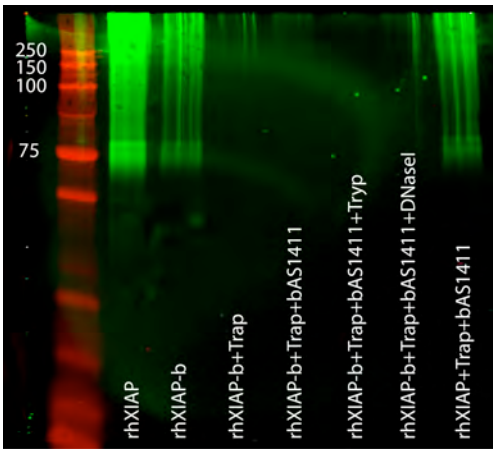

Biotinylated XIAP retains its capacity to inhibit caspase-7 activity
One measure of inhibition of apoptosis *in vivo* is the ability of XIAP-AS1411 complexes to inhibit caspase 7 activity. In order to assay the ability of biotinylated XIAP to inhibit caspase activity, we biotinylated XIAP and measured its ability to inhibit caspase 7.

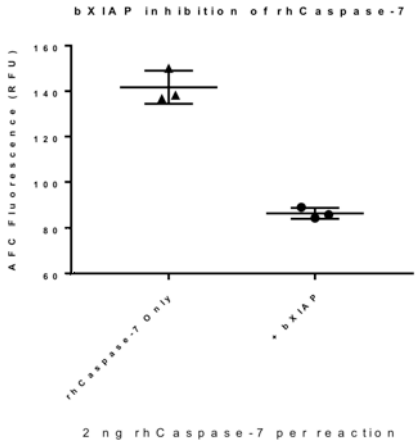

Opportunities for training and professional development:

The first author of the above two manuscripts (Derek Leaderer) completed the above studies as part of his PhD thesis, a requirement of the MSTP (MD/PhD) Program at Tufts University School of Medicine. The middle author, Dr. Siobhan Cashman is a junior faculty in my research program and she is currently under training to become an independent scientist. She is planning to submit her first NIH R01 grant application in 2017 as an independent investigator.

Dissemination: Through the above two published peer reviewed manuscripts

During the next period of our research we will complete the fourth and final goal of this study. In order to expedite completion of this goal we have recruited several additional research personnel into the study.

4. IMPACT

To our knowledge, the above technology is the first and only method currently available to efficiently deliver proteins into retinal cells (including photoreceptors) following intravitreal injection. While additional studies need to be completed, we believe the above technology is a platform that will impact studies in many fields over time.

Tufts University School of Medicine has been in communication with commercial entities in order to forge partnerships to potentially commercialize this technology.

5. CHANGES/PROBLEMS

There are no significant changes to the goals of our study. We have encountered a significant number of technical challenges that we have had to overcome, including use of alternative chemistries to those envisaged initially but we have successfully overcome each of our obstacles and the solutions to those obstacles are detailed in the accompanying manuscripts.

In order to complete our final and most important goal we have had to engage additional staff into this study than was originally intended but we are doing so by streamlining our studies such as not to impact our overall budget for this study.

There are no significant changes in use of vertebrate animals or biohazards.

6. PRODUCTS

The following two publications

G-quartet oligonucleotide mediated delivery of proteins into photoreceptors and retinal pigment epithelium via intravitreal injection.

Leaderer D, Cashman SM, Kumar-Singh R.

Experimental Eye Research. 2016 Apr;145:380-92. doi: 10.1016/j.exer.2016.02.009. Epub 2016 Feb 27.

We have found that the above technology is capable of inhibiting laser induced damage to the retina that leads to choroidal neovascularization (also a model of age related macular degeneration). This observation is published in the following manuscript:

Topical application of a G-Quartet aptamer targeting nucleolin attenuates choroidal neovascularization in a model of age-related macular degeneration.
Leaderer D, Cashman SM, Kumar-Singh R.

Exp Eye Res. 2015 Nov;140:171-8. doi: 10.1016/j.exer.2015.09.005. Epub 2015 Sep 12.

The technologies/ products are described in the above publications.

7. PARTICIPANTS AND OTHER COLLABORATING ORGANIZATIONS

Current:
Rajendra Kumar-Singh: PI,
Siobhan Cashman: Senior Staff, 6 months, organization and technical support, writing manuscripts, etc. 6 months on Ellison Foundation support.

Bhanu Dasari, Postdoctoral Fellow, 12 months; Chemistries for conjugation, technical support
Binit Kumar, Postdoctoral Fellow, 6 months; In vivo injections; characterization of proteins in the retina
Deepa Talreja, Postdoctoral Fellow, 12 months; Chemistries for conjugation and technical support
Vanessa Yanez, Graduate Student, 12 months; in vitro studies for macromolecule delivery

A change in active support:

One previous NIH grant has expired and we have been awarded a grant by DOD to further develop and test protein delivery for the retina.

Ongoing Research Support

W81XWH-16-1-0650 09/30/16-09/29/19
U.S. Army Medical Research Acquisition Activity
"Rapid Delivery of Protein Therapeutics into Retinal and Corneal Cells Following Intravitreal Injection"

The goals of this study are to develop a technology for the delivery of protein therapeutics for the retina and cornea
Role: PI

NIH R01EY026182 (PI Liddington) 01/14/2016- 01/31/2019
Interrogating the role of complement MAC in the pathogenesis of age-related macular degeneration: Structure- enhanced discovery of probes and leads for novel therapies
This is a subcontract ($50,157) from Sandford-Burnham Medical Research Institute to test small molecules for inhibition of MAC in laser induced choroidal neovascularization
PI Robert Liddington;
No scientific or funding overlap

ARM310- USArmy/ TATRC 8/30/12-8/29/16 (currently in no-cost extension)
Platform for the Rapid Delivery of Biologics and Drugs To Ocular Cells and Tissues Following Combat Associated Trauma
The goals of this study are to develop a technology for the delivery of protein therapeutics for the retina and cornea
Role: PI

PV3208- The Ellison Foundation 12/8/014-12/7/15 (currently in no-cost extension)
Gene Therapy for Age-Related Macular Degeneration (AMD)
This is a pilot project grant to develop sCD59 as a gene therapy for AMD.
Role: PI

Completed Research Support (last three years)

1R01EY021805 9/1/11 – 8/31/16
NIH/NEI
Non-Viral Gene Therapy for Retinal Degeneration
The goal of this study is to develop Peptide for Ocular Delivery (POD) for gene transfer to the retina as a tool for non-viral gene therapy

No other organization is currently involved as partner.

8. SPECIAL REPORTING REQUIREMENTS

Quad Chart Appended.

9. APPENDICES

Two manuscripts attached

Experimental Eye Research 145 (2016) 380–392

Contents lists available at ScienceDirect

Experimental Eye Research

journal homepage: www.elsevier.com/locate/yexer

Research article

G-quartet oligonucleotide mediated delivery of proteins into photoreceptors and retinal pigment epithelium via intravitreal injection

Derek Leaderer, Siobhan M. Cashman, Rajendra Kumar-Singh*

Department of Ophthalmology, Program in Genetics, Sackler School of Graduate Biomedical Sciences, Tufts University School of Medicine, 136 Harrison Avenue, Boston, MA 02111, USA

ARTICLE INFO

Article history:
Received 9 November 2015
Received in revised form
20 February 2016
Accepted in revised form 24 February 2016
Available online 27 February 2016

Keywords:
Aptamer
Retina
Cornea
Intravitreal
Topical
Nucleolin
Shuttle

ABSTRACT

There is currently no available method to efficiently deliver proteins across the plasma membrane of photoreceptor or retinal pigment epithelium (RPE) cells *in vivo*. Thus, current clinical application of recombinant proteins in ophthalmology is limited to the use of proteins that perform their biological function extracellularly. The ability to traverse biological membranes would enable the mobilization of a significantly larger number of proteins with previously well characterized properties. Nucleolin is abundantly present on the surface of rapidly dividing cells including cancer cells. Surprisingly, nucleolin is also present on the surface of photoreceptor cell bodies. Here we investigated whether nucleolin can be utilized as a gateway for the delivery of proteins into retinal cells following intravitreal injection. AS1411 is a G-quartet aptamer capable of targeting nucleolin. Subsequent to intravitreal injection, fluorescently labeled AS1411 localized to various retinal cell types including the photoreceptors and RPE. AS1411 linked to streptavidin (a ~50 kDa protein) via a biotin bridge enabled the uptake of Streptavidin into photoreceptors and RPE. AS1411-Streptavidin conjugate applied topically to the cornea allowed for uptake of the conjugate into the nucleus and cytoplasm of corneal endothelial cells. Clinical relevance of AS1411 as a delivery vehicle was strongly indicated by demonstration of the presence of cell surface nucleolin on the photoreceptors, inner neurons and ganglion cells of human retina. These data support exploration of AS1411 as a means of delivering therapeutic proteins to diseased retina.

1. Introduction

Delivery of biologically active proteins into retinal cells is hindered by the presence of multiple barriers. The current standard of care for delivery of proteins to the retina and retinal pigment epithelium (RPE) involves direct injection of the protein into the vitreous cavity (intravitreal injection) (Meyer et al., 2016). Because of the natural barriers associated with the plasma membrane, delivery of biologically active proteins to the retina is largely restricted to the use of molecules that function extracellularly, e.g. antibodies. Should efficient penetration of the plasma membrane by exogenously delivered proteins be possible, it would enable the mobilization of a large library of potentially therapeutic molecules including those that are only biologically active intracellularly. The impermeability of proteins by the plasma membrane can be overcome by the use of viral vectors for the delivery of genes coding for the exogenous protein (Thakur et al., 2014). However, transduction of photoreceptors or the RPE by a virus generally requires the vector to be injected into the subretinal space (Trapani et al., 2014; Carvalho and Vandenberghe, 2015) - a surgical procedure fraught with complications (Kim et al., 2014). Vector capsid modifications are currently being investigated to overcome this limitation and while much progress has been made, intravitreal delivery of viral vectors is generally not as efficient as subretinal delivery in the context of expressing exogenous proteins in photoreceptors and RPE (Trapani et al., 2014). Furthermore, recombinant viral vectors have some limitations including potential immunogenicity, limited transgene capacity and an inability to readily withdraw a therapy if necessitated by toxicity (Carvalho and Vandenberghe, 2015).

The current standard of care for the delivery of molecules to the cornea is via topical application. This procedure results in loss of the majority of the molecule via the lacrimal duct and leakage into

* Corresponding author.
E-mail address: Rajendra.Kumar-Singh@tufts.edu (R. Kumar-Singh).

http://dx.doi.org/10.1016/j.exer.2016.02.009
0014-4835/

systemic circulation (Rawas-Qalaji and Williams, 2012). Again, an efficient method of delivery of potentially therapeutic large molecules such as proteins to the corneal stroma *in vivo* is a currently unmet clinical need.

In order to address the above limitations, a variety of cell-penetrating proteins (CPPs) have been investigated as a means of delivering therapeutic biomolecules into ocular cells (Cashman et al., 2002, 2003; Kilic et al., 2004; Johnson et al., 2008, 2010; Read et al., 2010). These studies have had some success but efficient delivery of proteins to the photoreceptors or the RPE via intravitreal injection has thus far not been described. Moreover, as CPPs typically enter cells via endocytosis, much of their cargo becomes trapped and degraded in endosomes (Parnaste et al., 2015), resulting in limited bioavailability of the therapeutic molecule.

Nucleolin is an RNA and protein-binding protein involved in numerous cellular activities including rRNA maturation, ribosome assembly, mRNA metabolism, DNA replication and recombination (Tuteja and Tuteja, 1998). Nucleolin has also been implicated in many aspects of cell survival and proliferation (Tuteja and Tuteja, 1998). Nucleolin acts as a shuttle between the plasma membrane and the cytoplasm or the nucleus – a process occurring independently of the endosomes (Borer et al., 1989; Hovanessian et al., 2010). Although primarily a nuclear and cytoplasmic protein, elevated nucleolin has been observed on the cell membrane of mitotic cells, such as cancer cells (Hovanessian et al., 2010) and angiogenic endothelial cells (Hovanessian et al., 2000). Interestingly, cell surface nucleolin has also been observed on photoreceptors of both bovine and murine retina (Hollander et al., 1999; Conley and Naash, 2010), invoking the potential of cell surface nucleolin as a receptor for uptake of therapeutic molecules.

AS1411 is a G-quartet DNA aptamer that targets nucleolin (Bates et al., 2009). We have recently found that topical application of AS1411 can significantly reduce endothelial cell proliferation in the laser-induced model of choroidal neovascularization (Leaderer et al., 2015). In the present study, we investigate the presence of cell surface nucleolin, the target of AS1411, on cells of the murine, non-human primate and human retina. In addition, we describe the development of a platform technology utilizing AS1411 as a mode of delivering molecules, including fluorophore and exogenous protein to cells of the murine retina and cornea. Conjugation of AS1411 to fluorophore or streptavidin was used to determine the ability of AS1411 to deliver varying sizes of cargo to murine ocular cells *in vivo*. The proof of concept studies described herein indicate that surface nucleolin is present in murine, non-human primate and human retina and that AS1411 can successfully deliver both small and large molecules including protein to the retina and cornea *in vivo*.

2. Methods

2.1. Materials and reagents

AlexaFluor594 labeled AS1411 (FL-AS1411; 5′-FL-TTTGGTGGTGGTGGTTGTGGTGG TGGTGG-3′) and AlexaFluor594 labeled control oligonucleotide (FL-Control; 5′-FL-TTTATGT-CACCTCTATACGCCCCGGGCTG-3′) were synthesized by Invitrogen (Carlsbad, CA). All oligonucleotides were dissolved in nuclease free water. All other commercially available materials and reagents, including AlexaFluro594 labeled streptavidin (streptavidin^{594}), were purchased from Invitrogen, unless otherwise noted. Ocular cryosections from Cynomolgus monkey were obtained from Covance Laboratories (Dedham, MA). Normal human retina paraffin sections were purchased from Abcam (Cambridge, MA; Ab4364).

2.2. Streptavidin conjugates

4 nmols of biotinylated oligonucleotide was added to 1 nmol of streptavidin^{594} and allowed to incubate with gentle rocking at room temperature for 1 h. The resulting conjugates were then dialyzed with PBS using 30 K Ultrafree spin columns. The resultant conjugates were visualized on a native polyacrylamide gel stained with SybrGold (S11494).

2.3. Cellular uptake and localization

MCF7a cells were maintained in DMEM/F12 media supplemented with 5% fetal bovine serum (FBS). 24 h following seeding on a 96-well plate, MCF7a cells were washed twice with PBS and treated with 100 ng, 250 ng, 500 ng, or 1000 ng of streptavidin^{594}, control-streptavidin^{594} or AS1411-streptavidin^{594} conjugates diluted in DMEM/F12 supplemented with 2% FBS. Following a 1 h incubation at 37 °C, wells were washed 3 times with PBS and subsequently fixed with a 3.7% formaldehyde solution (Alfa Aesar; Ward Hill, MA).

2.4. AS1411-mediated delivery in vivo

Six to eight week old BALB/c males were purchased from Jackson Laboratories (Bar Harbor, ME, USA) and housed under a 12 h light/dark cycle, unless otherwise stated. Mice were cared for in accordance with federal, state and local regulations. Mice were anesthetized by intraperitoneal injection of 0.1 mg/g body weight Ketamine (Phoenix™, St Joseph, MO) and 0.01 mg/g body weight Xylazine (Lloyed, Shenandoah, Iowa), followed by topical application of 0.5% proparacaine hydrochloride (Akorn Inc., Lake Forest, IL, USA) to the cornea. Intravitreal injections were performed using a 32-gauge needle and a 5 μl glass syringe (Hamilton, Reno, NV, USA) using a transcleral approach proximal to the pars plana. A total volume of 1.5 μl containing 0.3 nmol of FL-AS1411 or FL-Control was injected for AS1411 localization experiments. For *in vivo* protein delivery, streptavidin^{594}, Control-streptavidin^{594} or AS1411-streptavidin^{594} conjugate was administered via intravitreal injection (1.5 μg) or topical application (5 μg). At various time-points post-injection/topical application, mice were sacrificed by CO_2 inhalation followed by cervical dislocation. Eyes were harvested, fixed in 4% paraformaldehyde, and dehydrated with a sucrose gradient. Frozen sections of retina and cornea were generated by embedding tissue in Optimal Cutting Temperature Compound (Sakura Finetek, Torrance, CA, USA) and sectioning at 12 μm using a Microm 550 Cryostat (Thermo Scientific, Rockford, IL, USA).

2.5. Immunohistochemistry

For nucleolin staining, fixed tissue sections and cell monolayers were incubated in 12% normal goat serum for 1 h followed by incubation with a 1:400 dilution of antibody against nucleolin (Abcam; ab22758) for 2.5 h at room temperature. Subsequent incubation with a Cy3-conjugated goat anti-rabbit antibody (1:200 dilution) for 1.5 h at room temperature was used for detection. Staining with Alexa Fluor488–conjugated Wheat Germ Agglutinin (WGA), a cell surface marker, was performed using a 1:200 dilution in PBS.

2.6. Imaging and statistics

Imaging was performed using an Olympus IX51 microscope equipped with a Retiga 2000r camera. Intensity of fluorescent signal was quantified from images using ImageJ software (National Institutes of Health; Bethesda, MD, USA). Confocal images were

captured using a Leica TCS SPE microscope (Leica Microsystems; Wetzlar, Germany).

Statistical analysis was performed using Prism 5 (GraphPad Software Inc, La Jolle, CA). Two-factor analysis of variance (ANOVA) was performed for *in vitro* streptavidin^{594} conjugation and dosing studies. Bonferroni's multiple comparison tests were used for Post hoc analysis. One-way analysis of variance (ANOVA) was performed for AS1411-streptavidin^{594}, Control-streptavidin^{594} and streptavidin^{594} topically treated corneas. Bonferroni's multiple comparison tests were used for Post hoc analysis.

3. Results

3.1. Nucleolin is present on the cell surface of BALB/c photoreceptors

Using an antibody specific for human and mouse nucleolin, retinal sections from BALB/c mice were probed for the presence of nucleolin. We identified nucleolin in the ganglion cell layer (GCL), the inner nuclear layer (INL), the outer nuclear layer (ONL) and the retinal pigment epithelium (RPE) of BALB/c mice (Fig. 1A(I)). The pattern of staining of the cell bodies in the ONL was significantly different to that of the other cell types. Specifically, the pattern of staining in the ONL was consistent with the presence of nucleolin on the cell surface (Fig. 1A(IV)), while that of the GCL, INL and RPE was consistent with cytoplasmic and/or nuclear localization of nucleolin (Fig. 1A(II, III, V)). In order to determine whether the staining of nucleolin in the ONL was consistent with localization at the cell surface, we co-stained the retinal sections with the cell surface marker, wheat germ agglutinin (WGA; Fig. 1B). The WGA-associated signal in the ONL (Fig. 1B(IV)) exhibited a similar pattern to that of nucleolin staining of the ONL (Fig. 1A(IV). An overlay of WGA and nucleolin signal of the ONL exhibited significant co-localization of nucleolin with WGA (Fig. 1C(IV)). However, consistent with previous studies of cell surface nucleolin (Chen et al., 2008a), the cell surface nucleolin signal in the ONL was observed to have a discontinuous, puncate distribution. Presence of cell surface nucleolin on the ONL of BALB/c retina is congruous with nucleolin distribution in the bovine and C57BL/6J murine retina (Hollander et al., 1999; Conley and Naash, 2010). Interestingly, no co-localization was observed between WGA and nucleolin staining in the GCL, INL and RPE of the BALB/c retina (Fig. 1C(II, III, V)), suggesting that the majority of the nucleolin detected in those cells was present in the nucleus and/or cytoplasm. This does not exclude the possibility that cell surface nucleolin is present at undetectable levels in these cells.

3.2. AS1411 localizes to a variety of ocular cell types after intravitreal delivery

AS1411 is a G-quartet oligonucleotide aptamer that has previously been shown to bind cell surface nucleolin (Bates et al., 2009). In order to determine whether retinal cells can bind and internalize AS1411, we injected 0.3 nmol of a fluorescently labeled AS1411 (FL-AS1411) or a fluorescently labeled control oligonucleotide (FL-Control) into the vitreous of adult BALB/c mice. Eyes were harvested at 4 h or at 24 h post-injection and processed for confocal microscopy.

At 4 h post-injection, confocal microscopy indicated a marked

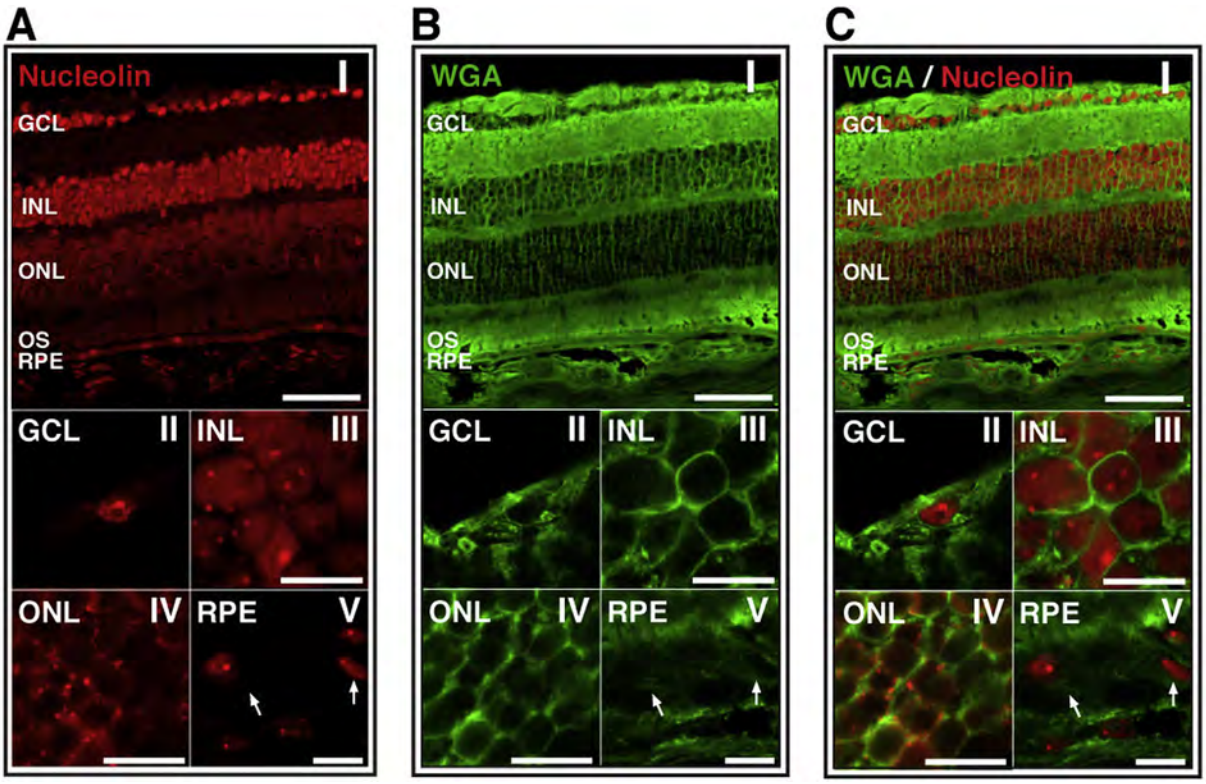

Fig. 1. Nucleolin is present on the surface of cells of the outer nuclear layer in BALB/c retina. (A) Confocal image of BALB/c retinal section stained for nucleolin; (I) whole retina, (II)–(V) increased magnification of GCL, INL, ONL and RPE, respectively. Arrows indicate the nuclei of RPE cells. (B) Confocal image of BALB/c retinal section stained with the cell surface marker, wheat germ agglutinin (WGA); (I) whole retina, (II)–(V) increased magnification of GCL, INL, ONL and RPE, respectively. Arrows indicate the cell surface of RPE cells. (C) Merged image of nucleolin and WGA staining indicates co-localization of these markers only on the ONL (yellow). Top panels scale bar = 60 μm; lower panels scale bar = 10 μm. *GCL, ganglion cell layer*; *INL, inner nuclear layer*; *ONL, outer nuclear layer*; *RPE, retinal pigment epithelium*. (For interpretation of the references to color in this figure legend, the reader is referred to the web version of this article.)

uptake of FL-AS1411 by the ONL, inner and outer segments (Fig. 2A(I, II)). Limited uptake of FL-AS1411 was observed in the GCL and INL (Fig. 2A(I, II)). At higher magnification, uptake of FL-AS1411 by the INL, ONL and RPE (Fig. 2A(IV–VI)) was evident. The increased level of uptake by the ONL relative to the GCL and INL is consistent with the presence of nucleolin on the surface of photoreceptor cell bodies (Fig. 1). Eyes injected intravitreally with FL-Control exhibited significantly less fluorescent signal in all retinal layers at 4 h (Fig. 2A). In addition, at this time-point FL-AS1411 was observed to localize to the endothelial, stromal and epithelial cell layers of the cornea (Fig. 2B). We could not exclude the possibility, that the FL-AS1411 observed in the epithelial cells occurs as a consequence of some leakage of FL-AS1411 during or immediately following ocular injection, rather than by trans-corneal transduction.

At 24 hours following intravitreal injection, confocal microscopy indicated that FL-AS1411 was taken up by the ONL, inner segments and RPE (Fig. 2C(I,II)). Higher magnification confocal images confirmed uptake by the ONL and RPE (Fig. 2C(V,VI)). In contrast, no fluorescence signal was detected in eyes injected with FL-Control at these same time points (Fig. 2C). At 24 h, FL-AS1411 was observed in the endothelial and stromal layers of the cornea, but considerably less fluorescence was observed in the epithelium than at 4 h (Fig. 2D).

3.3. AS1411 penetrates the cornea following topical delivery in vivo

Delivery of drugs into the cornea via topical application is inefficient, resulting in a considerable loss of drug to the systemic circulation (Rawas-Qalaji and Williams, 2012). In order to examine the potential of FL-AS1411 to act as a transporter of small molecules to the cornea following topical application, 1 nmol of FL-AS1411 or FL-control was administered to the cornea of BALB/c mice. Two hours following application, the corneas were harvested for examination. Fluorescence microscopy of whole corneas indicated considerable binding and possible uptake of FL-AS1411 relative to FL-Control (Fig. 3A). Quantification of the fluorescence intensity of the corneal flatmounts indicated an 8.02 ± 1.15 fold increase ($p = 0.002$) in signal intensity for FL-AS1411 treated eyes relative to FL-Control treated eyes (Fig. 3B). Images captured at higher magnification revealed a pattern of fluorescence consistent with cytoplasmic and nuclear localization of FL-AS1411 in corneal epithelial cells (Fig. 3C). Binding and possible uptake of FL-Control, although significantly less than that indicated for FL-AS1411, was also observed (Fig. 3A–C). Whether or not this uptake of FL-Control is receptor-mediated or due to a loss of membrane integrity by dying epithelial cells is not known. Some of the fluorescence observed on FL-Control treated corneas was consistent with a nuclear localization in corneal epithelial cells (Fig. 3C), but this occurred with much less efficiency relative to FL-AS1411 treated eyes. Optical sectioning of epithelial cells in the corneal flatmounts using confocal laser scanning microscopy confirmed uptake of FL-AS1411 in the cytoplasm and nucleus of epithelial cells (Fig. 3D). Transverse sections of treated corneas indicates FL-AS1411 to have permeated all layers of the cornea (Fig. 3E). FL-AS1411, although predominantly localized in the superficial layer of the epithelium, most likely squamous cells, was observed in the underlying basal and polygonal epithelial cells as well as the anterior limiting lamina, the stroma and the endothelium (Fig. 3E and F). This result was

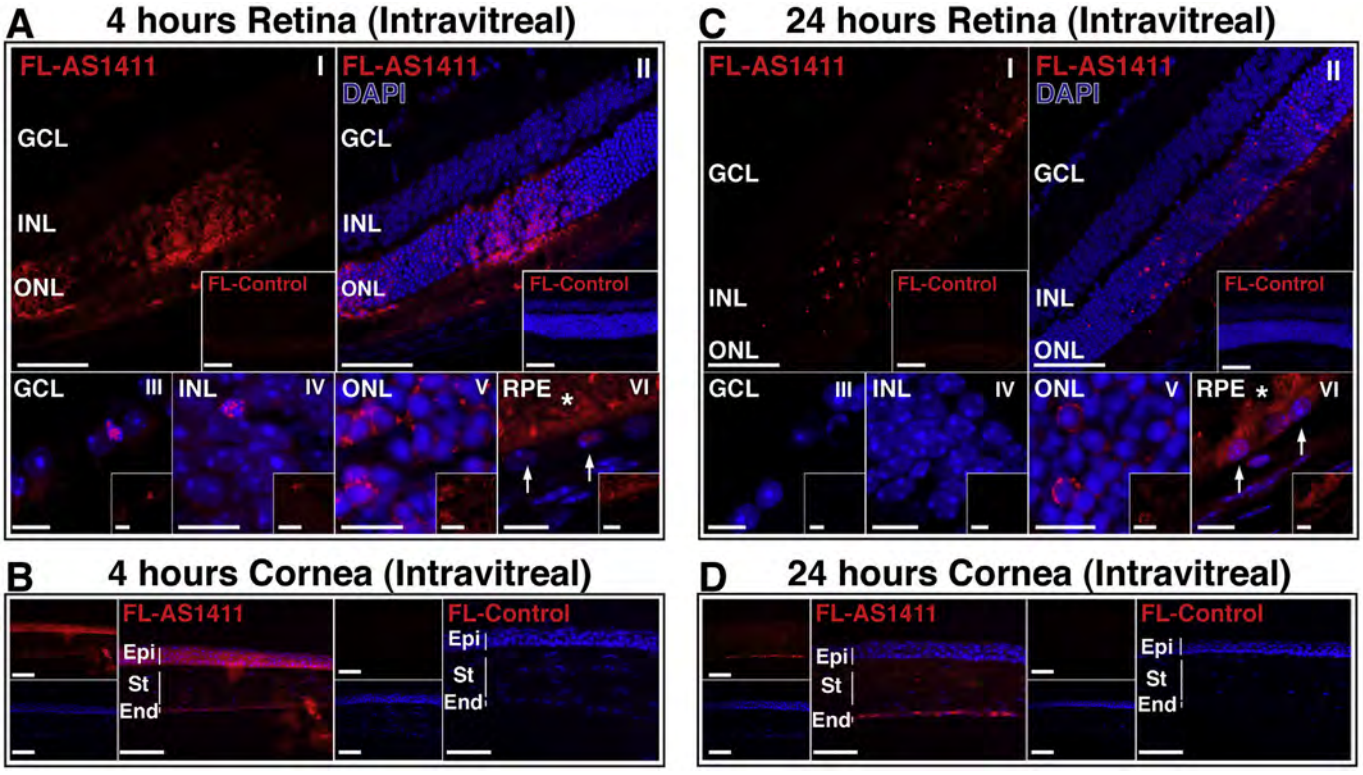

Fig. 2. AS1411 administered by intravitreal injection localizes to a variety of ocular cells in vivo. (A,C) Representative confocal images of BALB/c retina harvested 4 h and 24 h following intravitreal injection of 0.3 nmol AlexaFluro594 labeled AS1411 (FL-AS1411) or Control oligonucleotide (FL-Control; Insets). Top panels scale bar = 60 μm; lower panels scale bar = 10 μm; (I, II) whole retina, (III–VI) higher magnification of GCL, INL, ONL and RPE. Arrows indicate RPE nuclei; asterisk indicates outer segments. (B,D) Representative images of BALB/c cornea harvested 4 h and 24 h following intravitreal injection of 0.3 nmol FL-AS1411 or FL-Control. Scale bar = 60 μm. DAPI (blue) counterstains nuclei. n = 6 eyes/3 mice per condition/time point. *GCL-ganglion cell layer; INL-inner nuclear layer; ONL-outer nuclear layer; RPE-retinal pigment epithelium; Epi-epithelium; St-stroma; End-endothelium.* (For interpretation of the references to color in this figure legend, the reader is referred to the web version of this article.)

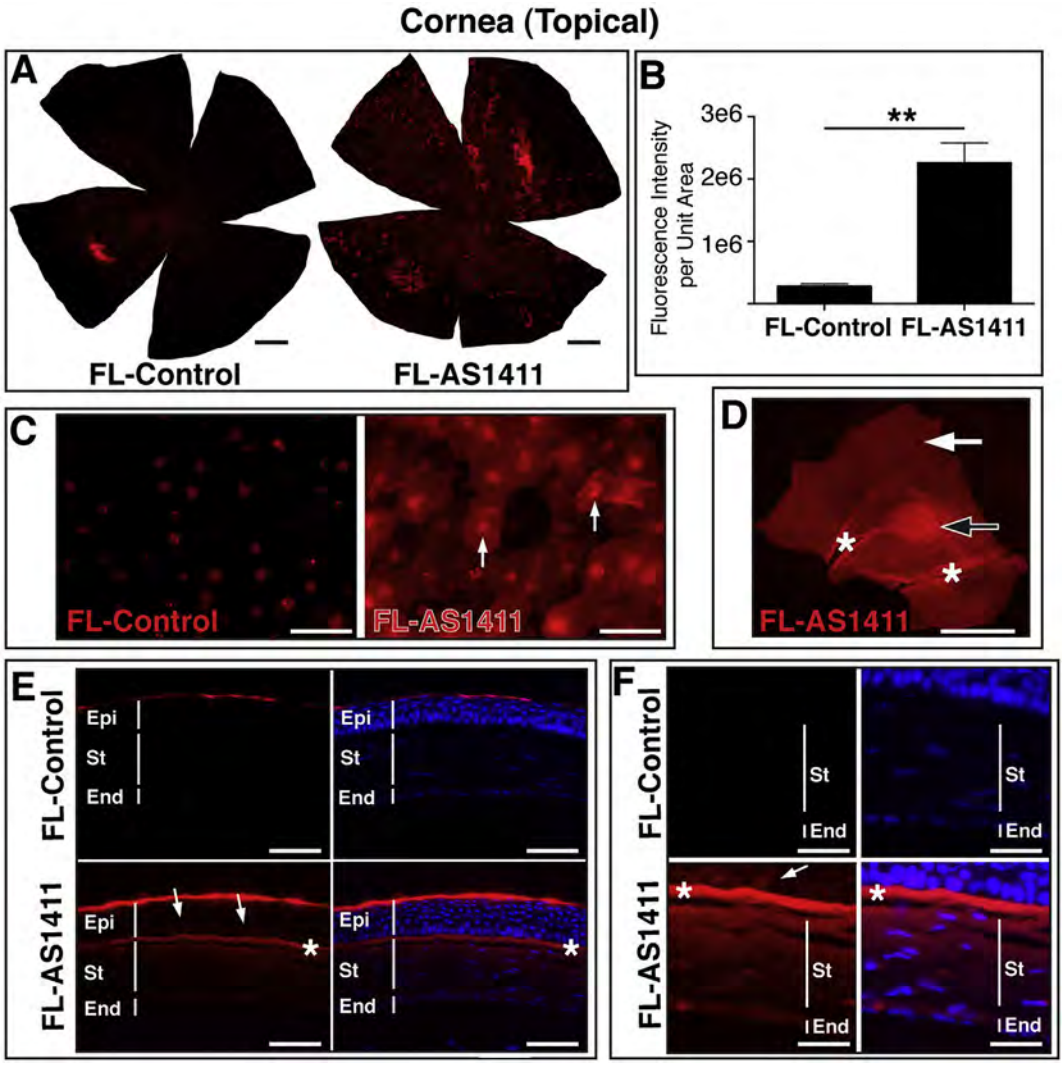

Fig. 3. Topical application of AS1411 results in uptake by corneal cells *in vivo*. (A) Representative corneal flat mounts harvested 2 h post topical application of 1 nmol FL-AS1411 or FL-Control [scale bar = 0.5 mm]. (B) Quantitation of fluorescent signal per area of topically treated corneas ($p = 0.002$, $n = 6$ for each of FL-AS1411, FL-Control). (C) Higher magnification of flat mounts from FL-AS1411 or FL-Control treated cornea. Scale bar = 60 μm. Arrows indicate nuclear localization. (D) A representative image from a series of confocal laser scanned micrographs of a corneal epithelial cell showing FL-AS1411 in the nucleus (black/white arrow) and cytoplasm (white arrow). Asterisks indicate areas of wrinkling, typical of superficial epithelial cells. Scale bar = 20 μm. (E) Transverse sections of corneas topically treated with FL-AS1411 or FL-Control shows FL-AS1411 in all layers of the cornea. Basal and polygonal cells of the epithelium are indicated by arrows. FL-Control was observed only in the superficial squamous cell layer of the epithelium. Asterisks indicate the anterior limiting lamina. Scale bar = 60 μm. (F) Higher magnification of the deeper layers of the epithelium, the stroma and the endothelium show FL-AS1411 permeation of these layers, while FL-Control is undetectable. Scale bar = 30 μm n = 4 eyes/2 mice for each of FL-AS1411, FL-Control. *Epi-epithelium*; *St-stroma*; *End-endothelium*.

unexpected, since tight junctions present in the superficial epithelial layer are known to prevent molecules from passing into the cornea. Localization of the FL-Control oligonucleotide within the corneal epithelium, was also observed in transverse sections of control treated corneas, but was limited to the surface (squamous cell) layer (Fig. 3E and F).

3.4. AS1411 can deliver protein into cells in vitro

In order to determine whether AS1411 can also deliver larger molecules such as proteins across the plasma membrane, we tested the ability of AS1411 to deliver fluorophore-conjugated streptavidin (streptavidin^{594}), an ~50 kDa protein into MCF7a cells *in vitro*. We conjugated streptavidin^{594} to either biotinylated AS1411 (AS1411-streptavidin^{594}) or to biotinylated control oligonucleotide (Control-streptavidin^{594}). In order to examine the conjugate, the reaction products were electrophoresed in parallel with the unconjugated reagents through a native polyacrylamide gel. The AS1411 aptamer was detected in the gel using SybrGold, whereas the streptavidin^{594} was visualized by its fluorescent label (Fig. 4A). As anticipated with successful conjugation, we observed a shift in migration of the AS1411-conjugated streptavidin^{594} (AS1411-streptavidin^{594}; Fig. 4A, lane 3) relative to both the unconjugated streptavidin^{594} (Fig. 4A, lane 2) and the biotinylated AS1411 (Fig. 4A, lane 1). The same shift in migration was observed for the control oligonucleotide conjugated streptavidin^{594} (Control-streptavidin$^{594;}$ Fig. 4A, lane 6) relative to the unconjugated streptavidin^{594} (Fig. 4A, lane 5) and the biotinylated control oligonucleotide (Fig. 4A, lane 4). Interestingly, the AS1411-Streptavidin^{594} and Control-streptavidin^{594} conjugates (Fig. 4A, lanes 3 and 6) exhibited an accelerated migration through the gel relative to the unconjugated streptavidin^{594} (lanes 2 and 5). This is possibly due to the conjugation of the DNA that increases the net negative charge of the conjugate. To examine this, the AS1411-Streptavidin^{594} and

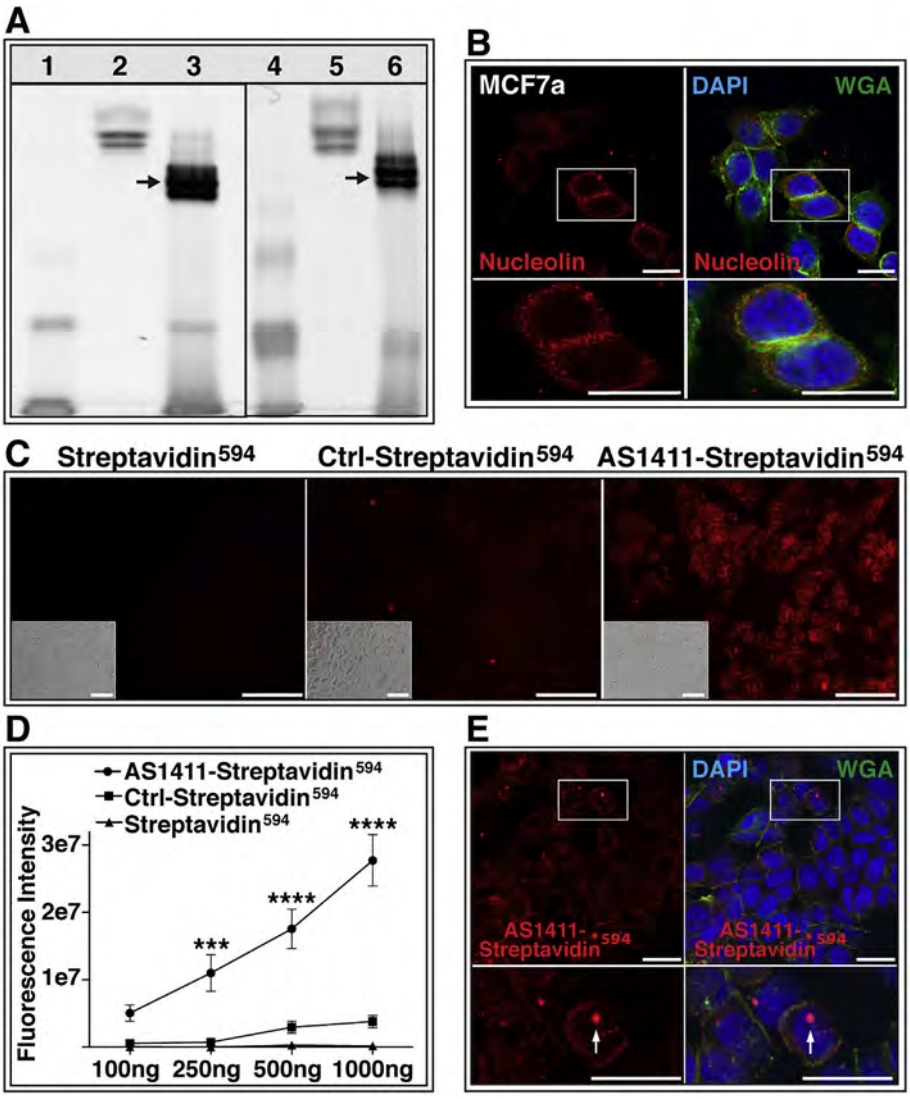

Fig. 4. AS1411 delivers protein to cells in vitro. (A) Native polyacrylamide gel confirms conjugation of streptavidin^{594} with biotinylated AS1411. Lane 1: biotinylated AS1411; Lanes 2 and 5: Streptavidin^{594}; Lane 3: AS1411-Streptavidin^{594} conjugate; Lane 4: biotinylated control oligonucleotide; Lane 6: Control-Streptavidin^{594} conjugate;. Arrows indicate conjugation products. (B) MCF7a cells probed with antibody against nucleolin (red) or stained with wheat germ agglutinin (WGA; green) and DAPI (blue). Scale bar = 20 μm (C) MCF7a cells incubated for 1 h with 1000 ng of Streptavidin^{594}, Ctrl-Streptavidin^{594}, or AS1411-Streptavidin^{594}. Bright-field images shown in insert. Scale bar = 120 μm. (D) Quantification of raw fluorescence intensity of MCF7a cells incubated with increasing doses of Streptavidin^{594}, Ctrl-Streptavidin^{594}, or AS1411-Streptavidin^{594} (study performed twice in triplicate) (*** = $p < 0.001$; **** = $p < 0.0001$). (E) Confocal microscopy of AS1411-Streptavidin^{594} (red) incubated cells stained with WGA (green) and DAPI (blue). Arrow indicates nuclear localization of AS1411-Streptavidin^{594}. Scale bar = 20 μm. *Ctrl-Control*. (For interpretation of the references to color in this figure legend, the reader is referred to the web version of this article.)

Control-streptavidin^{594} conjugates were incubated with DNAse I and shown to exhibit a migration pattern similar to unconjugated streptavidin^{594} (data not shown). Collectively, these results suggest efficient conjugation of AS1411 or Control oligonucleotide with streptavidin^{594}.

MCF7a is a breast cancer derived cell line previously shown to express cell surface nucleolin (Litchfield et al., 2012). Confocal microscopy of non-permeabilized MCF7a cells stained for both nucleolin and WGA exhibited co-localization of these markers, confirming the presence of nucleolin on the cell surface (Fig. 4B). Incubation of MCF7a cells with 1000 ng AS1411-Streptavidin^{594} for 1 h resulted in a significantly greater binding and potential uptake of streptavidin^{594} than did incubation of MCF7a cells with either Control-streptavidin^{594} or unconjugated streptavidin^{594} (Fig. 4C). A two-factor analysis of variance of the fluorescence intensity of treated MCF7a cells indicated both a dose dependence and a significant effect of the AS1411 conjugation on streptavidin^{594} targeting of MCF7a cells, in addition to a significant interaction between the two variables ($p < 0.0001$; Fig. 4D). A significantly increased fluorescence intensity of AS1411-streptavidin^{594} incubated cells was observed with 250 ng ($p < 0.001$), 500 ng ($p < 0.0001$) and 1000 ng ($p < 0.0001$) relative to that of Control-streptavidin^{594} and streptavidin^{594} incubated cells. No significant difference in fluorescence intensity was observed between Control-streptavidin^{594} and streptavidin^{594} incubated cells for any of the doses examined (Fig. 4D). Confocal microscopy performed on AS1411-streptavidin^{594} incubated MCF7a cells confirmed internalization of the AS1411-streptavidin^{594} conjugate and demonstrated its localization to both the cytoplasm and the nucleus (Fig. 4E).

3.5. AS1411 mediates delivery of protein to retinal cells in vivo

We next examined if AS1411 could deliver streptavidin^{594} into retinal cells *in vivo*. Six-week-old BALB/c mice were administered 1.5 μg of either AS1411-streptavidin^{594}, Control-streptavidin^{594} or streptavidin^{594} via intravitreal injection. Eyes were harvested at 4 h and 24 h post-injection. At 4 h post-injection, a marked binding of AS1411-streptavidin^{594} by a variety of retinal tissues was observed (Fig. 5A). At 4 h, the strongest binding of AS1411-streptavidin^{594} was observed on the RPE, the outer and inner segments (IS/OS) and the outer plexiform layer (OPL), with moderate binding of the ONL and little or no binding of the INL and GCL (Fig. 5A). This pattern of staining was consistent with the binding pattern of fluorophore labeled AS1411 (Fig. 2A). Little or no binding of either Control-streptavidin^{594} or unconjugated streptavidin^{594} was noted in the ONL, INL and GCL at this same time point. Some minor binding of the unconjugated streptavidin^{594} was observed on the RPE – possibly due to the presence of endogenous biotin (Wang and Pevsner, 1999) – but this was considerably less than that observed for the AS1411-streptavidin^{594}. No binding of the RPE was observed for the Control-streptavidin^{594}. Confocal microscopy of the retinal tissues harvested at 4 h post-injection revealed uptake of AS1411-streptavidin^{594} by the strongly bound tissues – the RPE, IS/OS and OPL - as well as uptake by both the ONL and INL (Fig. 5B). Despite the limited binding of AS1411-streptavidin^{594} by the GCL at 4 h (Fig. 5A), confocal microscopy revealed an intense fluorescent signal in the nerve fiber layer of the GCL (Fig. 5B, asterisks). The majority of AS1411-streptavidin^{594} taken up by the RPE, ONL and INL was localized to the cytoplasm (Fig. 5B). AS1411-streptavidin^{594} was detected also in the nuclei of RPE cells and the INL (Fig. 5B, *arrows*), but at considerably lower levels than in the cytoplasm.

At the 24 h time-point, a considerable reduction of AS1411-streptavidin^{594} signal was observed on the IS/OS and OPL (Fig. 5A) relative to that observed at 4 h. Although reduced relative to 4 h, an intense AS1411-streptavidin^{594} signal was still noted in the RPE at 24 h (Fig. 5A). Neither the Control-streptavidin^{594} or unconjugated streptavidin^{594} showed detectable fluorescent signal in any retinal tissue at this time point (Fig. 5A). Confocal microscopy of the retinal tissues harvested at 24 h confirmed these findings. AS1411-streptavidin^{594} was still strongly present in the RPE, in both the cytoplasm and nucleus (Fig. 5B). While the ONL and INL had little or no detectable AS1411-streptavidin^{594} at this time point, the conjugate was still detectable within the GCL and OPL.

Considering the potential for corneal transduction by AS1411 (Fig. 2B,D), we also analyzed the corneas at 4 and 24 h following intravitreal injection. At 4 h post injection, AS1411-streptavidin^{594} was observed in both the endothelium and throughout the stroma of the cornea (Fig. 6A). At 24 h, strong fluorescent signal was still observed in both of these corneal layers (Fig. 6B). Counterstain with DAPI suggested uptake of AS1411-streptavidin^{594} by the nucleus of stromal fibroblasts at 4 h (Fig. 6A) and both stromal fibroblasts and corneal endothelial cells at 24 h (Fig. 6B). There was no detectable transduction of cornea following intravitreal injection of Control-streptavidin^{594} or Streptavidin^{594} at either the 4 h (Fig. 6A) or 24 h (Fig. 6B) timepoints.

3.6. Topical application of AS1411-strepatividin^{594} results in uptake by corneal cells

Due to the considerable potential impact of topical delivery of

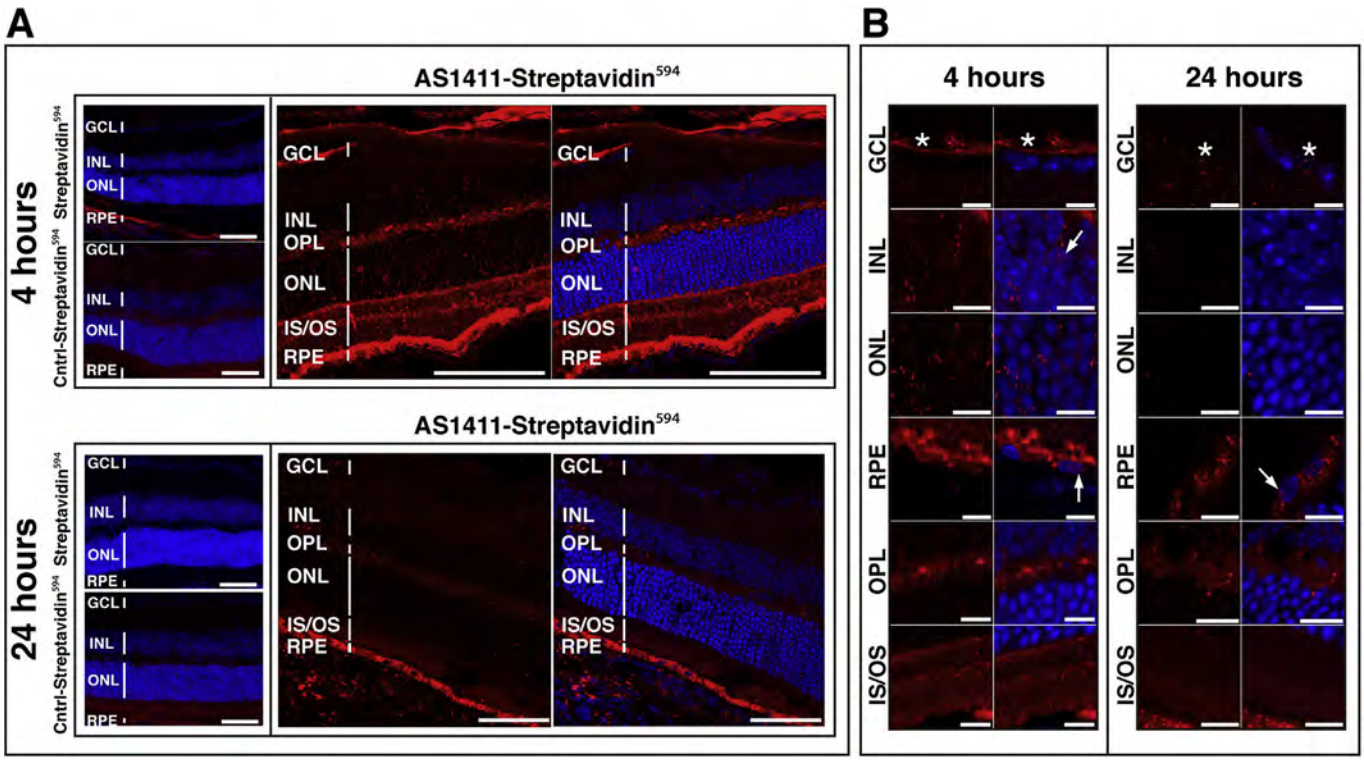

Fig. 5. AS1411-Streptavidin^{594} transduces mouse retinal cells following intravitreal injection. (A) Sections of BALB/c retina harvested 4 h and 24 h following intravitreal injection of 1.5 μg of either AS1411-Streptavidin^{594}, Control-Streptavidin^{594}, or unconjugated Streptavidin^{594}. Sections were counterstained with DAPI (blue; n = 6 eyes/3 mice per condition/time point). Scale bar = 60 μm. (B) Confocal microscopy of retinal sections at 4 and 24 h following intravitreal delivery of AS1411-Streptavidin^{594}. Scale bar = 10 μm. Asterisks indicate nerve fiber layer. Arrows indicate red fluorescence signal in the nucleus. *Cntrl-Control; GCL-ganglion cell layer; INL-inner nuclear layer; ONL-outer nuclear layer; IS/OS-inner/outer segments; RPE-retinal pigment epithelium; OPL-outer plexiform layer.* (For interpretation of the references to color in this figure legend, the reader is referred to the web version of this article.)

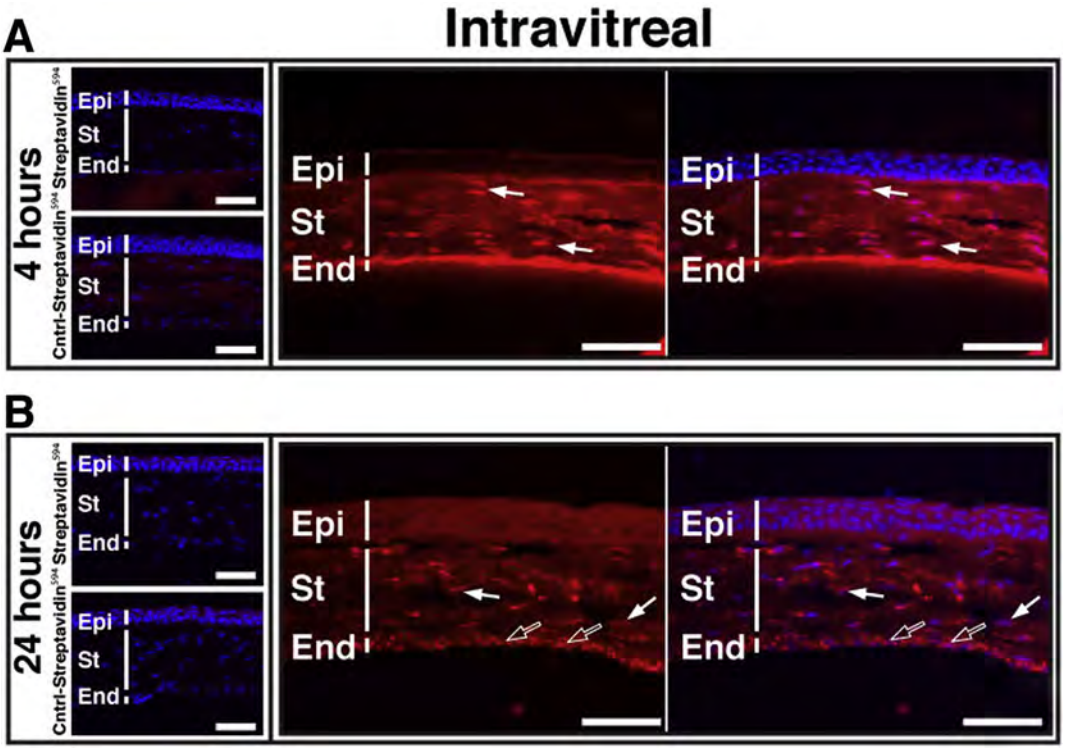

Fig. 6. AS1411-Streptavidin^{594} transduces mouse cornea following intravitreal injection. Corneal sections of BALB/c eyes harvested (A) 4 h and (B) 24 h following intravitreal injection of 1.5 μg of either AS1411-Streptavidin^{594}, Control-Streptavidin^{594} or Streptavidin^{594}. Scale bar = 60 μm. Arrows indicate nuclear localization (solid arrows, stromal fibroblasts; hollow arrows, endothelial cells). *Cntrl-control; Epi-epithelium; St-stroma; End-endothelium.*

drugs for the treatment of ocular diseases, we next determined whether AS1411 could deliver a 50 kDa protein such as streptavidin into mouse cornea following topical application. We administered 5 μg of either AS1411-streptavidin^{594}, Control-streptavidin^{594} or streptavidin^{594} to the cornea of 6 week-old male BALB/c mice. Two hours following topical application, the eyes were harvested and corneas examined for transduction. Fluorescence microscopy of whole cornea flatmounts indicated a markedly enhanced binding with possible uptake by corneas treated with AS1411-streptavidin^{594} compared to corneas treated with Control-streptavidin^{594} or streptavidin^{594} (Fig. 7A). Quantification of the fluorescence intensity of streptavidin^{594} conjugates on the corneal flatmounts indicated that AS1411-streptavidin^{594} treated corneas had bound 3.76 ± 0.87 fold and 3.92 ± 0.86 fold ($p < 0.001$ for both) more strepatividin^{594} than Control-streptavidin^{594} and streptavidin^{594} treated corneas, respectively (Fig. 7B). While some binding and/or uptake of streptavidin^{594} was observed in both Control-streptavidin^{594} and streptavidin^{594} treated corneas (Fig. 7A), consistent with binding of FL-control to cornea following topical delivery (Fig. 3A,B), the amount of streptavidin^{594} did not differ significantly between these groups.

At higher magnification, the pattern of fluorescence on the AS1411-streptavidin^{594} treated corneas was observed to be consistent with nuclear localization (Fig. 7C, *arrows*). Confocal microscopy of AS1411-streptavidin^{594} treated corneal flatmounts confirmed nuclear uptake of the conjugate (Fig. 7D). Unlike the FL-AS1411, transverse sections of treated corneas revealed that the AS1411-streptavidin^{594} applied topically to the cornea was delivered almost exclusively to corneal epithelial cells (Fig. 7E), likely due to the presence of tight junctions between the epithelial cells (Eghrari et al., 2015) preventing passage of larger molecules through the cornea. At the corneal limbus (peripheral cornea), however, AS1411-strepatividin^{594} could be observed throughout the stroma and endothelium (Fig. 7F). Whether this is due to structural differences at the corneal limbus or a non-uniform dispersion of the topically applied "drop" over the corneal surface is not known.

3.7. Cell surface nucleolin is present on neurons of non-human primate retina

While mammalian retinas share a significant degree of homology, there are significant differences between murine and primate retina, most notably the absence of a macula in the murine retina (Volland et al., 2015). To assess the potential of AS1411 as a delivery vehicle for primate retina, transverse sections of retina of Cynomolgus monkey *(Macaca fascicularis)* were probed for the presence of nucleolin using a polyclonal anti-nucleolin antibody (Fig. 8). Presence of nucleolin on the cell surface was determined by co-staining with WGA. Non-human primate retinal cells stained strongly positive for nucleolin in the GCL, INL, ONL and RPE of both the central (Fig. 8A) and peripheral (Fig. 8D) retina. To determine localization and make a qualitative assessment of WGA and nucleolin, optical sectioning of retinal sections using confocal microscopy was performed. In the central retina, we observed limited overlap between WGA and nucleolin, indicating an intracellular and predominantly nuclear localization of nucleolin in the GCL and RPE (Fig. 8A–C). In both the INL and ONL of the central retina, some co-localization of WGA and nucleolin was observed (Fig. 8C, arrows), indicating presence of nucleolin on the surface of these cells, but a majority of the nucleolin appeared to occur intracellularly.

In the peripheral retina, observation of limited co-localization of WGA and nucleolin indicated a predominantly cytoplasmic and nuclear localization of nucleolin in the GCL and RPE (Fig. 8D), similar to that of the GCL and RPE of the central retina (Fig. 8A). Unlike the observations for the central retina, however, the GCL of

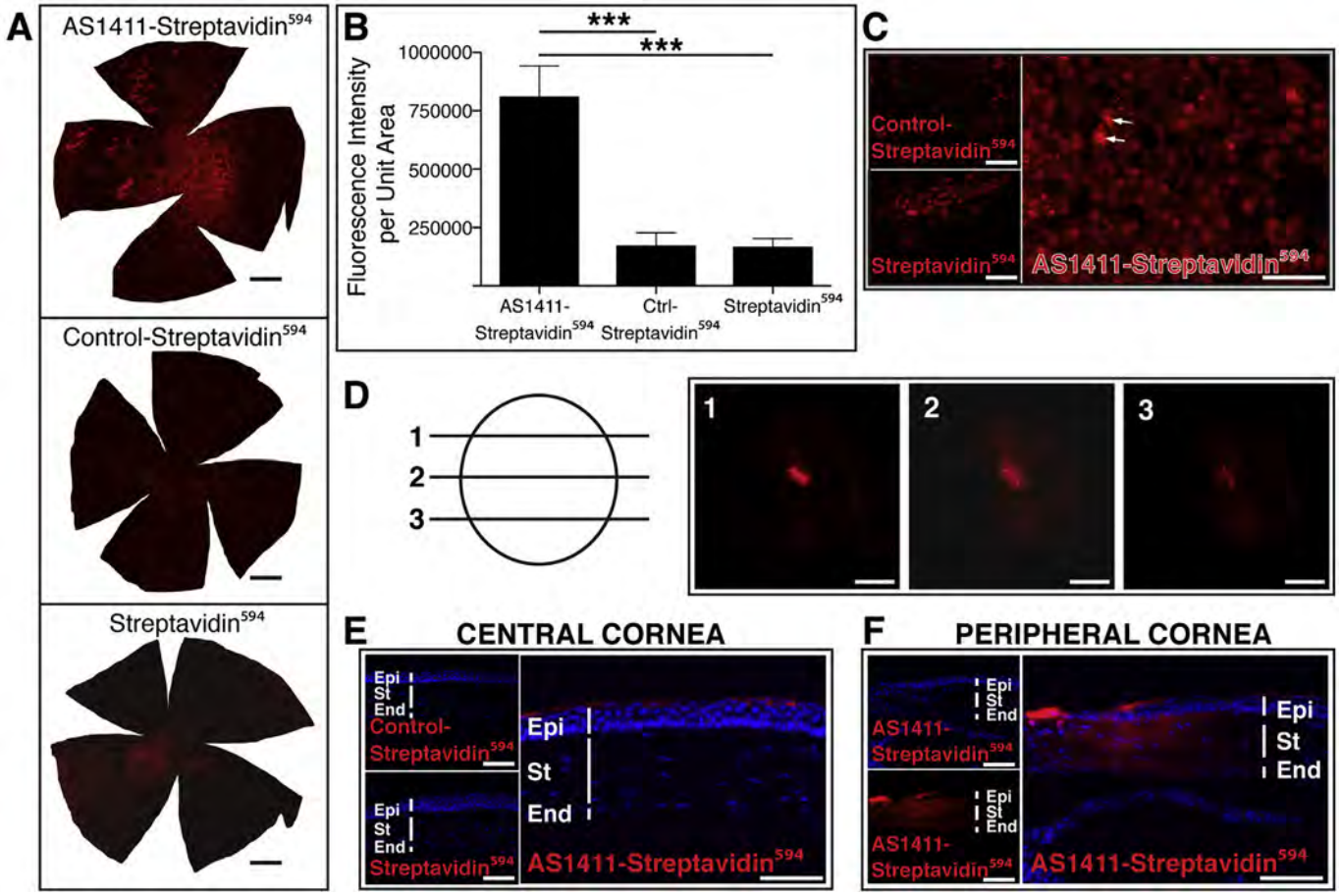

Fig. 7. Topical Application of AS1411-streptavidin^{594} results in uptake by corneal cells and nuclear localization *in vivo*. (A) Corneal flat mounts harvested 2 h post topical application of 5 μg of AS1411-Streptavidin^{594}, Control-Streptavidin^{594} or Streptavidin^{594}. Scale bar = 0.5 mm. (B) Quantitation of the intensity of fluorescence of streptavidin^{594} conjugates per area of corneal flatmount (n = 6 per condition, *** = $p < 0.001$). (C) Higher magnification images of AS1411-Streptavidin^{594}, Control-Streptavidin^{594} or Streptavidin^{594} treated corneal flat mounts. Scale bar = 120 μm. Arrows indicate examples of nuclear binding. (D) Confocal series of a flatmount of AS1411-Streptavidin^{594} treated cornea indicating nuclear localization within a corneal epithelial cell. Scale bar = 20 μm. (E) Transverse sections of corneas treated topically with AS1411-Streptavidin^{594}, Control-Streptavidin^{594} or Streptavidin^{594} (n = 4 eyes/2 mice per condition). Scale bar = 60 μm. (F) Transverse section of AS1411-strepatividin^{594} treated cornea showing transduction of stroma and endothelium at the corneal limbus. Scale bar = 60 μm. *Ctrl-Control; Epi-epithelium; St-stroma; End-endothelium.*

the peripheral retina showed strong nucleolin staining in both the cytoplasm and nucleus (Fig. 8F). There was little or no co-localization of nucleolin with WGA in either the GCL or RPE of the peripheral retina (Fig. 8E, F), indicating little surface nucleolin. The INL and ONL of the peripheral retina exhibited a pattern of nucleolin staining (Fig. 8D) very similar to that of WGA in these cells (Fig. 8E), consistent with presence of nucleolin on the surface of these cells (Fig. 8F).

3.8. Cell surface nucleolin is present in all neuronal layers of adult human retina

To further investigate the clinical potential of AS1411 for retinal drug delivery, we determined the distribution of nucleolin in the adult human retina. Human retinal sections stained for nucleolin exhibited the presence of nucleolin in the GCL, INL, ONL and RPE (Fig. 9A). Co-staining of retinal sections with WGA (Fig. 9B), suggested strong co-localization of nucleolin and WGA in the INL, ONL and GCL (Fig. 9C).

4. Discussion

In recent years, there has been a significant interest in the use of aptamers as drug delivery agents (Zhu et al., 2015). Aptamers can be designed to have a strong affinity for targets, extended shelf life, low immunogenicity and cost-efficient identification and synthesis. *Pegaptanib*, an aptamer targeting VEGF, has been approved by the FDA for the treatment of Age-related Macular Degeneration (Gragoudas et al., 2004). Phase II of a clinical study has just been completed for the nucleolin-targeting aptamer, AS1411, investigating efficacy as a therapy for Acute Myeloid Leukemia (https://clinicaltrials.gov/ct2/show/NCT00512083). We have recently found the potential of AS1411 delivered by either intravitreal injection or by topical application to inhibit choroidal neovascularization in a murine model of AMD (Leaderer et al., 2015). To our knowledge this is the first study, however, demonstrating the use of an aptamer as a protein delivery system in the eye.

Previously, cell-penetrating peptides (CPP) have been utilized for ocular delivery of fluorophore and protein (Cashman et al., 2003; Johnson et al., 2010; Binder et al., 2011). HIV-derived TAT and herpes simplex virus-derived VP22 peptides function efficiently *in vitro*, but have considerably reduced efficiency *in vivo* (Cashman et al., 2002, 2003; Kilic et al., 2004). Likely due to a paucity of alternatives, the TAT CPP continues to be investigated as a vehicle for delivery of ocular therapies (Zhang et al., 2015; Ozaki et al., 2015). Peptide for ocular delivery (POD) can deliver cargo to

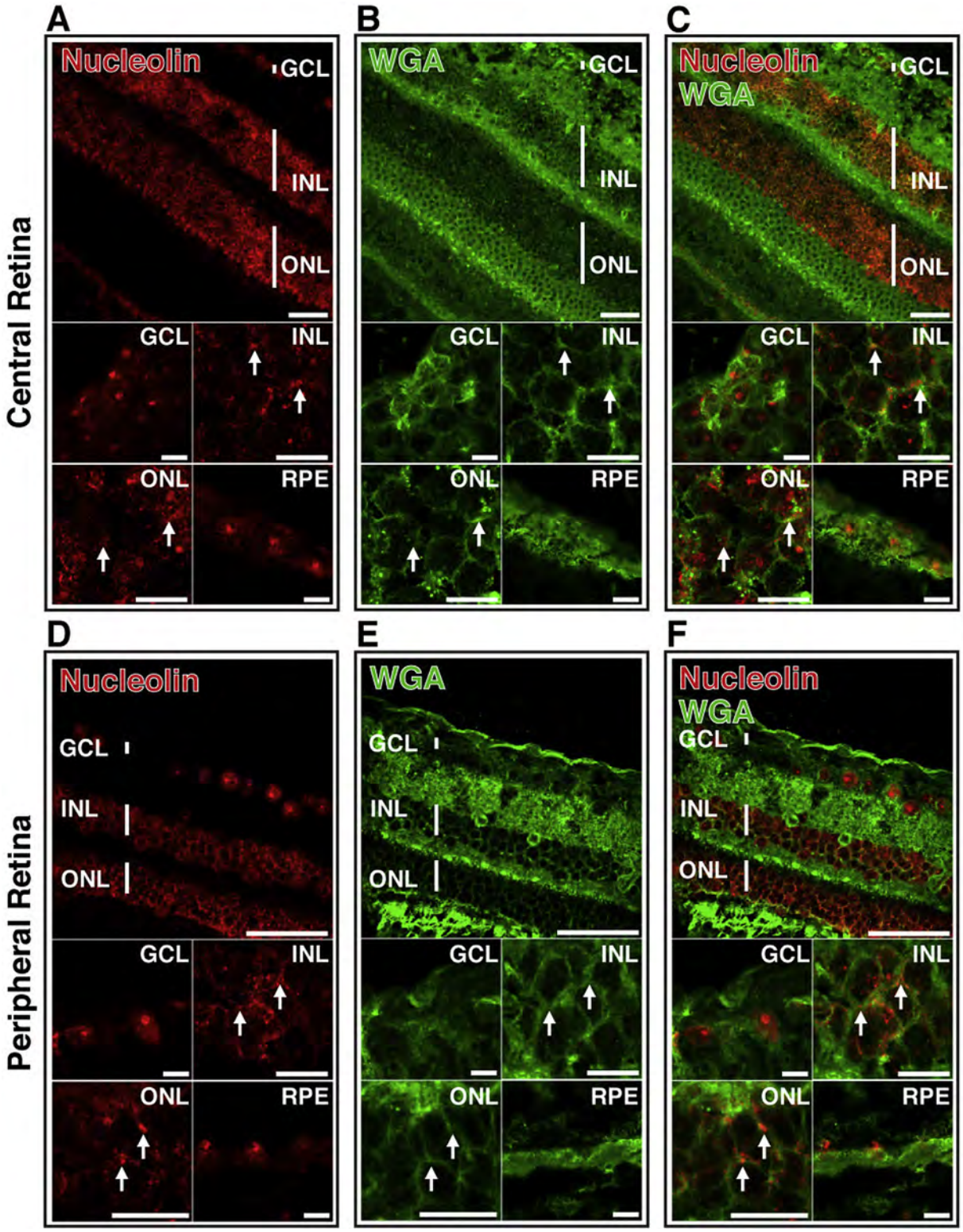

Fig. 8. Cell surface nucleolin is present on neurons of non-human primate retina. Confocal microscopy of retinal sections of Cynomolgus monkey (*macaca fascicularis*) stained with anti-nucleolin antibody (A,D; red) and WGA (B,E; green). Images from both central and peripheral retina are shown. Overlay of images A and B (C) and D and E (F) indicates co-localization of nucleolin and WGA (yellow). Arrows indicate regions of co-localization. Top panels scale bar = 60 μm; lower panels scale bar = 10 μm. *GCL-ganglion cell layer; INL-inner nuclear layer; ONL-outer nuclear layer; RPE-retinal pigment epithelium.* (For interpretation of the references to color in this figure legend, the reader is referred to the web version of this article.)

murine photoreceptors and RPE following subretinal delivery, but upon intravitreal administration, transduction is almost exclusively of ganglion cells (Johnson et al., 2008, 2010). In contrast, herein we found that AS1411 aptamer injected intravitreally in mice can

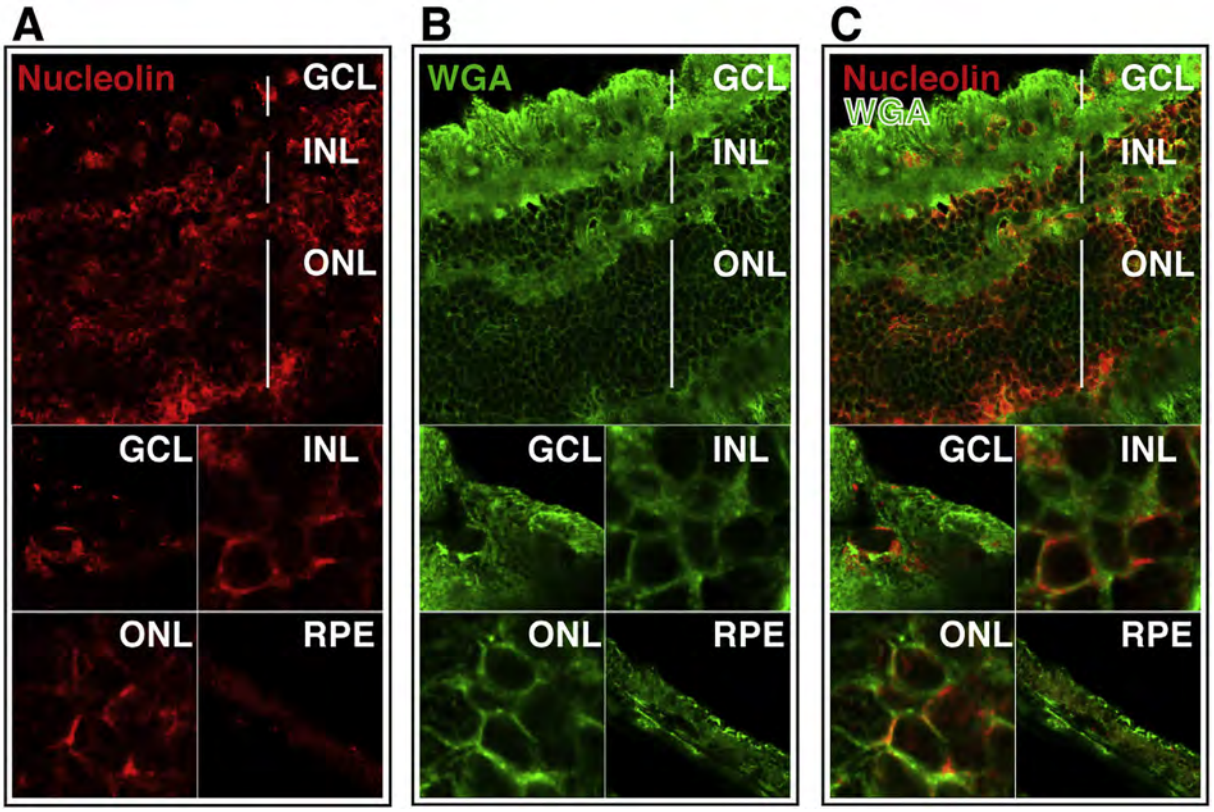

Fig. 9. Cell surface nucleolin is present in all neuronal layers of adult human retina. Confocal images of sections of human retina probed with anti-nucleolin antibody (A; red) and WGA (B; green). Overlay of images A and B (C) indicates co-localization of nucleolin and WGA (yellow). Top panels scale bar = 60 μm; lower panels scale bar = 10 μm. *GCL-ganglion cell layer*; *INL-inner nuclear layer*; *ONL-outer nuclear layer*; *RPE-retinal pigment epithelium*. (For interpretation of the references to color in this figure legend, the reader is referred to the web version of this article.)

deliver an ~50 kDa protein to the cytoplasm and nucleus of photoreceptors and the RPE. Intravitreal administration of AS1411 also enabled uptake of the 50 kDa protein by the endothelium and stroma of the cornea. Furthermore, topical application of the AS1411 conjugate enabled uptake by the nucleus of corneal epithelial cells, as well as delivery to the stroma and endothelium at the corneal limbus. Uptake of AS1411-strepavidin^{594} *in vitro* occurs in a dose-dependent manner and results in delivery to the nucleus. Collectively, these results strongly indicate the potential for AS1411 as a transporter of proteins or other cargo to the RPE, retinal neurons, and cells of the cornea.

Aptamers are currently being used as delivery vehicles for therapeutic conjugates in liver, solid tumors, T lymphocytes and bone tissue (Zhu et al., 2015). In addition, the conjugated therapeutics tested have included a wide range of molecules – chemotherapeutics, photosensitizing agents, siRNAs and enzymes (Zhu et al., 2015). The AS1411 aptamer, in addition to the above, has been used to deliver oligonucleotides (Kotula et al., 2012), antibody complexes (Park et al., 2012), as well as polymer- (Aravind et al., 2012; Guo et al., 2011), protein- (Wu et al., 2013), and liposome-based (Kim et al., 2012; Liao et al., 2015) nanoparticles of up to ~200 nm to a variety of cell types *in vitro* and *in vivo*. AS1411-coated cell membrane capsules of >900 nm efficiently delivered a chemotherapeutic to xenograft tumors following intravenous injection in mice (Peng et al., 2015), resulting in a 2.2-fold reduction in tumor growth relative to a 1.3-fold reduction in tumor size following injection of uncoated capsules of the same agent. Similar results were observed for AS1411-conjugated liposomes carrying doxorubicin when injected intravenously in tumor grafted mice, in which a significant inhibition of tumor growth, side effects of the drug – specifically, cardiotoxicity – was observed relative to injection of unconjugated liposomes (Liao et al., 2015). This was likely due to increased targeting of the chemotherapeutic agent to the tumor, with reduced accumulation in other tissues. Nanoparticles conjugated with AS1411 and without the addition of chemotherapeutic agent have themselves been shown to slow growth of liver tumors *in vivo* to a modest degree (Zhang et al., 2014).

While much use has been made, however, of AS1411 as a targeting agent for a variety of molecules *in vivo*, to our knowledge all of these studies have involved delivery to tumors. Our study is, therefore, the first to demonstrate the use of AS1411 as a delivery agent to terminally-differentiated, non-dividing cells *in vivo*. The focus on tumors prior to our study is likely due to the significant literature describing the presence of cell surface nucleolin on proliferating rather than quiescent cells (Hovanessian et al., 2000, 2010). However, a number of studies in addition to that presented herein, have demonstrated the presence of nucleolin on the surface of photoreceptor cell bodies of both murine and bovine retina (Hollander et al., 1999; Conley and Naash, 2010). The capacity of AS1411 to deliver molecules differing from streptavidin in size, charge and composition to non-mitotic cells of the retina remains to be demonstrated. However, delivery of streptavidin to cells *in vitro* by an RNA aptamer, has been shown to be a reliable indicator of the aptamer's capacity to deliver a functional lysosomal enzyme (Chen et al., 2008b). Unlike the endosomal dependent, transferrin-binding RNA aptamer (Chen et al., 2008b), AS1411 enters cells through a cell surface nucleolin binding pathway (Bates et al., 2009) that has been previously found to be capable of

transporting nanoparticles directly to the nuclei of cells in a pathway independent of endosomes (Chen et al., 2008a).

Delivery of AS1411 conjugates to murine photoreceptors *in vivo* following intravitreal injection is consistent with the presence of nucleolin exclusively on the ONL of murine retina (Fig. 1). In addition, the significant potential of AS1411 for delivery of protein to photoreceptors of human retina is strongly indicated by nucleolin staining of the cell surface of the ONL of both non-human primate and human retina. Interestingly, equivalent staining for nucleolin was also observed on the cell surface of inner neurons in both non-human primate and human retina, extending potential application of AS1411-mediated delivery of protein to inner retinal neurons. These results suggest that while some similarities of nucleolin localization occur between species, the retinal distribution of nucleolin is, somewhat, species-specific. However, the presence of cell surface nucleolin in all neuronal layers of the human retina bodes favorably for the use of AS1411 as a mode of drug delivery for human retinal diseases.

While this mode of treatment may require repeated injections, intravitreal injection is a current standard of clinical care found to be relatively safe and well tolerated (Meyer et al., 2016). For example, many patients being treated for the “wet” form of AMD receive intravitreal injections every 4–6 weeks (Stewart, 2015).

In the murine retina, intravitreal injection of AS1411-streptavidin^{594} also led to localization of the conjugate in the RPE. This hints at the potential use of AS1411-meditated delivery of therapeutic proteins for the treatment of diseases associated with degeneration of RPE cells, such as in age-related macular degeneration. The uptake of AS1411-streptavidin^{594} by murine RPE, however, was not consistent with the observation that nucleolin was not detectable on the surface of RPE cells in either the murine or primate retina. Thus, it is possible that the AS1411-streptavidin^{594} conjugate was phagocytosed by the RPE either directly or as a constituent of photoreceptor outer segments (Kevany and Palczewski, 2010). This hypothesis is supported by the observation that AS1411-mediated uptake of both fluorophore and protein significantly increases at the later (24-h) time-point after injection, a time when the amount of AS1411 cargo in the ONL and outer segment is seen to be reduced (Figs. 2 and 5).

Topical delivery of drugs to the cornea is highly inefficient, resulting in a considerable loss of drug to the systemic circulation (Rawas-Qalaji and Williams, 2012). Topical delivery of AS1411-streptavidin^{594} resulted in efficient uptake of AS1411 by corneal epithelial cells. Conjugation of AS1411 to existing topical treatments may increase the bioavailability of these compounds and allow for less “off target” effects.

In conclusion, our study suggests that AS1411 can efficiently deliver a prototypical protein of ~50 kDa to the nuclei and cytoplasm of a variety of retinal and corneal cells, and that AS1411 employs cell surface nucleolin to deliver its cargo. The presence of surface nucleolin on inner and outer neurons of non-human primate and human retina strongly indicates the potential of AS1411 for delivery of conjugates to human retina and favors further exploration of AS1411 as a delivery vehicle for treatments of a variety of ocular diseases.

Acknowledgments

This study was supported by grants to R.K.S from The Department of Defense/TATRC, The Paul and Phyllis Fireman Foundation and The National Institute of Health/NEI (EY021805 and EY013837).

References

Aravind, A., Jeyamohan, P., Nair, R., et al., 2012. AS1411 aptamer tagged PLGA-lecithin-PEG nanoparticles for tumor cell targeting and drug delivery. Biotechnol. Bioeng. 109, 2920–2931.
Bates, P.J., Laber, D.A., Miller, D.M., Thomas, S.D., Trent, J.O., 2009. Discovery and development of the G-rich oligonucleotide AS1411 as a novel treatment for cancer. Exp. Mol. Pathol. 86, 151–164.
Binder, C., Read, S.P., Cashman, S.M., Kumar-Singh, R., 2011. Nuclear targeted delivery of macromolecules to retina and cornea. J. Gene Med. 13, 158–170.
Borer, R.A., Lehner, C.F., Eppenberger, H.M., Nigg, E.A., 1989. Major nucleolar proteins shuttle between nucleus and cytoplasm. Cell 56, 379–390.
Carvalho, L.S., Vandenberghe, L.H., 2015. Promising and delivering gene therapies for vision loss. Vis. Res. 111, 124–133.
Cashman, S.M., Sadowski, S.L., Morris, D.J., Frederick, J., Kumar-Singh, R., 2002. Intercellular trafficking of adenovirus-delivered HSV VP22 from the retinal pigment epithelium to the photoreceptors–implications for gene therapy. Mol. Ther. 6, 813–823.
Cashman, S.M., Morris, D.J., Kumar-Singh, R., 2003. Evidence of protein transduction but not intercellular transport by proteins fused to HIV tat in retinal cell culture and in vivo. Mol. Ther. 8, 130–142.
Chen, X., Kube, D.M., Cooper, M.J., Davis, P.B., 2008. Cell surface nucleolin serves as receptor for DNA nanoparticles composed of pegylated polylysine and DNA. Mol. Ther. 16, 333–342.
Chen, C.H., Dellamaggiore, K.R., Ouellette, C.P., et al., 2008. Aptamer-based endocytosis of a lysosomal enzyme. Proc. Natl. Acad. Sci. U. S. A. 105, 15908–15913.
Conley, S.M., Naash, M.I., 2010. Nanoparticles for retinal gene therapy. Prog. Retin. Eye Res. 29, 376–397.
Eghrari, A.O., Riazuddin, S.A., Gottsch, J.D., 2015. Overview of the cornea: structure, function, and development. Prog. Mol. Biol. Transl. Sci. 134, 7–23.
Gragoudas, E.S., Adamis, A.P., Cunningham Jr., E.T., Feinsod, M., Guyer, D.R., 2004. Pegaptanib for neovascular age-related macular degeneration. N. Engl. J. Med. 351, 2805–2816.
Guo, J., Gao, X., Su, L., et al., 2011. Aptamer-functionalized PEG-PLGA nanoparticles for enhanced anti-glioma drug delivery. Biomaterials 32, 8010–8020.
Hollander, B.A., Liang, M.Y., Besharse, J.C., 1999. Linkage of a nucleolin-related protein and casein kinase II with the detergent-stable photoreceptor cytoskeleton. Cell Motil. Cytoskelet. 43, 114–127.
Hovanessian, A.G., Puvion-Dutilleul, F., Nisole, S., et al., 2000. The cell-surface-expressed nucleolin is associated with the actin cytoskeleton. Exp. Cell Res. 261, 312–328.
Hovanessian, A.G., Soundaramourty, C., El Khoury, D., Nondier, I., Svab, J., Krust, B., 2010. Surface expressed nucleolin is constantly induced in tumor cells to mediate calcium-dependent ligand internalization. PLoS One 5, e15787.
Johnson, L.N., Cashman, S.M., Kumar-Singh, R., 2008. Cell-penetrating peptide for enhanced delivery of nucleic acids and drugs to ocular tissues including retina and cornea. Mol. Ther. 16, 107–114.
Johnson, L.N., Cashman, S.M., Read, S.P., Kumar-Singh, R., 2010. Cell penetrating peptide POD mediates delivery of recombinant proteins to retina, cornea and skin. Vis. Res. 50, 686–697.
Kevany, B.M., Palczewski, K., 2010. Phagocytosis of retinal rod and cone photoreceptors. Physiol. (Bethesda) 25, 8–15.
Kilic, U., Kilic, E., Dietz, G.P., Bahr, M., 2004. The TAT protein transduction domain enhances the neuroprotective effect of glial-cell-line-derived neurotrophic factor after optic nerve transection. Neurodegener. Dis. 1, 44–49.
Kim, J.K., Choi, K.J., Lee, M., Jo, M.H., Kim, S., 2012. Molecular imaging of a cancer-targeting theragnostics probe using a nucleolin aptamer- and microRNA-221 molecular beacon-conjugated nanoparticle. Biomaterials 33, 207–217.
Kim, Y.C., Chiang, B., Wu, X., Prausnitz, M.R., 2014. Ocular delivery of macromolecules. J. Control Release 190, 172–181.
Kotula, J.W., Pratico, E.D., Ming, X., Nakagawa, O., Juliano, R.L., Sullenger, B.A., 2012. Aptamer-mediated delivery of splice-switching oligonucleotides to the nuclei of cancer cells. Nucleic Acid Ther. 22, 187–195.
Leaderer, D., Cashman, S.M., Kumar-Singh, R., 2015. Topical application of a G-Quartet aptamer targeting nucleolin attenuates choroidal neovascularization in a model of age-related macular degeneration. Exp. Eye Res. 140, 171–178.
Liao, Z.X., Chuang, E.Y., Lin, C.C., et al., 2015. An AS1411 aptamer-conjugated liposomal system containing a bubble-generating agent for tumor-specific chemotherapy that overcomes multidrug resistance. J. Control Release 208, 42–51.
Litchfield, L.M., Riggs, K.A., Hockenberry, A.M., et al., 2012. Identification and characterization of nucleolin as a COUP-TFII coactivator of retinoic acid receptor beta transcription in breast cancer cells. PLoS One 7, e38278.
Meyer, C.H., Krohne, T.U., Charbel Issa, P., Liu, Z., Holz, F.G., 2016. Routes for drug delivery to the eye and retina: intravitreal injections. Dev. Ophthalmol. 55, 63–70.
Ozaki, T., Nakazawa, M., Yamashita, T., Ishiguro, S., 2015. Delivery of topically applied calpain inhibitory peptide to the posterior segment of the rat eye. PLoS One 10, e0130986.
Park, S., Hwang, D., Chung, J., 2012. Cotinine-conjugated aptamer/anti-cotinine antibody complexes as a novel affinity unit for use in biological assays. Exp. Mol. Med. 44, 554–561.
Parnaste, L., Arukuusk, P., Zagato, E., Braeckmans, K., Langel, U., 2015. Methods to follow intracellular trafficking of cell-penetrating peptides. J. Drug Target 1–12.
Peng, L.H., Zhang, Y.H., Han, L.J., et al., 2015. Cell membrane capsules for encapsulation of chemotherapeutic and cancer cell targeting in vivo. ACS Appl. Mater. Interfaces 7 (33), 18628–18637.
Rawas-Qalaji, M., Williams, C.A., 2012. Advances in ocular drug delivery. Curr. Eye

Res. 37, 345–356.
Read, S.P., Cashman, S.M., Kumar-Singh, R., 2010. POD nanoparticles expressing GDNF provide structural and functional rescue of light-induced retinal degeneration in an adult mouse. Mol. Ther. 18, 1917–1926.
Stewart, M.W., 2015. Individualized treatment of neovascular age-related macular degeneration: what are patients gaining? or losing? J. Clin. Med. 4, 1079–1101.
Thakur, S.S., Barnett, N.L., Donaldson, M.J., Parekh, H.S., 2014. Intravitreal drug delivery in retinal disease: are we out of our depth? Expert Opin. Drug Deliv. 11, 1575–1590.
Trapani, I., Puppo, A., Auricchio, A., 2014. Vector platforms for gene therapy of inherited retinopathies. Prog. Retin. Eye Res. 43, 108–128.
Tuteja, R., Tuteja, N., 1998. Nucleolin: a multifunctional major nucleolar phosphoprotein. Crit. Rev. Biochem. Mol. Biol. 33, 407–436.
Volland, S., Esteve-Rudd, J., Hoo, J., Yee, C., Williams, D.S., 2015. A comparison of some organizational characteristics of the mouse central retina and the human macula. PLoS One 10, e0125631.
Wang, H., Pevsner, J., 1999. Detection of endogenous biotin in various tissues: novel functions in the hippocampus and implications for its use in avidin-biotin technology. Cell Tissue Res. 296, 511–516.
Wu, J., Song, C., Jiang, C., Shen, X., Qiao, Q., Hu, Y., 2013. Nucleolin targeting AS1411 modified protein nanoparticle for antitumor drugs delivery. Mol. Pharm. 10, 3555–3563.
Zhang, B., Luo, Z., Liu, J., Ding, X., Li, J., Cai, K., 2014. Cytochrome c end-capped mesoporous silica nanoparticles as redox-responsive drug delivery vehicles for liver tumor-targeted triplex therapy in vitro and in vivo. J. Control Release 192, 192–201.
Zhang, X., Li, Y., Cheng, Y., et al., 2015. Tat PTD-endostatin: a novel anti-angiogenesis protein with ocular barrier permeability via eye-drops. Biochim. Biophys. Acta 1850, 1140–1149.
Zhu, G., Niu, G., Chen, X., 2015. Aptamer-drug conjugates. Bioconjugate Chem. 26 (11), 2186–2197.

Experimental Eye Research 140 (2015) 171–178

Contents lists available at ScienceDirect

Experimental Eye Research

journal homepage: www.elsevier.com/locate/yexer

Research article

Topical application of a G-Quartet aptamer targeting nucleolin attenuates choroidal neovascularization in a model of age-related macular degeneration

Derek Leaderer, Siobhan M. Cashman, Rajendra Kumar-Singh*

Department of Developmental, Molecular and Chemical Biology, Program in Genetics, Sackler School of Graduate Biomedical Sciences, Tufts University School of Medicine, 136 Harrison Avenue, Boston, MA 02111, USA

ARTICLE INFO

Article history:
Received 26 March 2015
Received in revised form
8 August 2015
Accepted in revised form 9 September 2015
Available online 12 September 2015

Keywords:
AS1411
Laser-induced choroidal neovascularization (CNV)
Nucleolin
Age-related macular degeneration (AMD)
Aptamer

ABSTRACT

Choroidal neovascularization (CNV) associated with the 'wet' form of age related macular degeneration (AMD) is one of the most common causes of central vision loss among the elderly. The 'wet' form of AMD is currently treated by intravitreal delivery of anti-VEGF agents. However, intravitreal injections are associated with complications and long-term inhibition of VEGF leads to macular atrophy. Thus, there is currently an unmet need for the development of therapies for CNV that target molecules other than VEGF. Here, we describe nucleolin as a novel target for the 'wet' form of AMD. Nucleolin was found on the surface of endothelial cells that migrate from the choroid into the subretinal space in the laser-induced model of 'wet' AMD. AS1411 is a previously described G-quartet oligonucleotide that has been shown to bind nucleolin. We found that AS1411 inhibited the formation of tubes by human umbilical vein endothelial cells (HUVECs) by approximately 27.4% *in vitro*. AS1411 co-localized with the site of laser induced CNV *in vivo*. Intravitreally injected AS1411 inhibited laser-induced CNV by 37.6% and attenuated infiltration of macrophages by 40.3%. Finally, topical application of AS1411 led to a 43.4% reduction in CNV. Our observations have potential implications for the development of therapies for CNV and specifically for the 'wet' form of AMD.

1. Introduction

Age related macular degeneration (AMD) is the leading cause of central vision loss in developed nations among individuals 65 years of age and older (Lim et al., 2012). An advanced form of AMD known as 'wet' AMD involves the growth of new blood vessels from the choroid into the subretinal space (choroidal neovascularization or CNV) (Bhutto and Lutty, 2012). These new blood vessels are generally immature and hence leak fluids into the retina, causing macular edema (Bhutto and Lutty, 2012). CNV in AMD patients is associated with an elevation of vascular endothelial growth factor (VEGF) and thus, anti-VEGF antibodies including *ranibizumab* and *bevacizumab* are the current standard of care for the treatment of 'wet' AMD (Funk et al., 2009; Saint-Geniez et al., 2009; Ferrara, 2010; Martin et al., 2011). However, anti-VEGF antibodies need to be injected into the ocular compartment via intravitreal injection every four to twelve weeks (Keane and Sadda, 2012). Repeated intravitreal injections are associated with endophthalmitis, retinal detachment and increased intraocular pressure (Sampat and Garg, 2010). Although the frequency of these complications is relatively low per injection, these frequencies become relevant over the lifetime of the patient. Moreover, given that AMD affects primarily an aged population, the relatively high frequency of intraocular injections negatively impacts patient compliance (Goldstein et al., 2012).

Recent clinical studies confirm prior studies in animals suggesting that long-term inhibition of VEGF is deleterious to the retina (Nishijima et al., 2007; Papadopoulou et al., 2009; Sacu et al., 2011; Kurihara et al., 2012; Campochiaro et al., 2014). Specifically, an anti-VEGF mediated regression of CNV can lead to macular atrophy (Campochiaro et al., 2014). This observation is not surprising given that VEGF is involved in a large variety of cellular processes including maintenance of tissue homeostasis (Saint-Geniez et al., 2008). Delivery of VEGF-inhibitors to the eye can also lead to systemic complications in some individuals due to anti-VEGF antibodies traveling from the ocular compartment into systemic

* Corresponding author.
E-mail address: Rajendra.Kumar-Singh@tufts.edu (R. Kumar-Singh).

http://dx.doi.org/10.1016/j.exer.2015.09.005
0014-4835/

circulation (Heiduschka et al., 2007; Ueta et al., 2009, 2011). Thus, there is currently an unmet need for the development of inhibitors of CNV that target molecules other than VEGF. There is also an unmet need for a mechanism of drug delivery for anti-CNV agents that is less invasive than intravitreal injections.

The most commonly used animal model for the 'wet' form of AMD is laser induced CNV. In this model, a laser burn of the Bruch's membrane causes a local elevation of VEGF and a subsequent migration of endothelial cells from the choroid into the subretinal space, features observed in 'wet' AMD patients (Lambert et al., 2013). Despite some limitations, this model of 'wet' AMD is widely used for the testing and development of novel inhibitors of CNV.

Nucleolin is a ubiquitously expressed phosphoprotein involved in numerous cellular activities, including rRNA maturation, ribosome assembly and mRNA metabolism (Abdelmohsen and Gorospe, 2012). Despite being a nuclear and cytoplasmic protein, nucleolin is also found on the surface of various cancer cells (Hovanessian et al., 2000, 2010; Abdelmohsen and Gorospe, 2012). Surface nucleolin serves as a receptor for various growth factors such as midkine and lactoferrin (Legrand et al., 2004; Hovanessian, 2006). AS1411 is a G-quartet quadruplex DNA aptamer formed from a single strand G-rich phosphodiester oligonucleotide (Bates et al., 1999). AS1411 has been found to have various anti-proliferative effects including cell cycle arrest of cancer cells via binding to cell surface nucleolin (Bates et al., 2009). We wished to test the hypothesis that nucleolin is expressed on the surface of endothelial cells migrating from the choroid into the subretinal space following laser induced injury. We also wished to test the hypothesis that AS1411 may inhibit the formation of such CNV when delivered to the intravitreal compartment. Finally, we wished to test the hypothesis that topical application of AS1411 to the ocular surface may also inhibit laser induced CNV. If successful, our studies will have identified a drug target not previously implicated in an animal model of AMD. Equally important, our results will address the clinically relevant need of development of drugs that can inhibit CNV without the need for an invasive intravitreal injection.

2. Materials and methods

2.1. Materials

The oligodeoxynucelotides AS1411, (5′-d(GGTGGTGGTGGTTGTGGTGGTGGTGG)-3′), and inactive control oligonucleotide CRO, 5′-d(CCTCCTCCTCCTTCTCCTCCTCCTCC)-3′ were synthesized by the Tufts Core DNA Synthesis facility (Tufts University, Boston, MA). AlexaFluro594 labeled AS1411, 5′-FL-AS1411, and AlexaFluro594 labeled CRO, 5′-FL-CRO, were purchased from Invitrogen and used for localization studies. All oligonucleotides were dissolved in nuclease free water. Neutralizing goat antibody against mouse VEGF-A (AF-493) was purchased from R&D Systems (Minneapolis, MN) and 2 pmol were administered via intravitreal injection for lasered mice.

2.2. Endothelial Tube Formation Assay

Tube formation assays were completed according to the Endothelial Tube Formation Assay (*In Vitro* Angiogenesis) protocol as per manufacture's instructions (Life Technologies Corporation, Carlsbad, CA). 4.5×10^4 HUVECs were seeded per well of a 24-well plate on Geltrex™ (Reduced Growth Factor Basement Membrane Matrix, Life Technologies Corporation, Carlsbad, CA) coated wells. Incubations were performed by adding CRO or AS1411 to 200PRF/LSGS medium to a final concentration of 500 nM. 200PRF/LSGS medium was used as a positive control. 18 h post-incubation, microscopic images of each well were captured (IX51, Olympus, Center Valley, PA) and the number of master junctions, master segments and meshes determined using the "HUVEC angiogenesis analyzer plugin" for ImageJ software. Master segments are defined as tube segments between two junctions each of which contain 2 additional branches. Master junctions are defined as junctions linking at least 3 master segments and meshes are defined as areas enclosed by segments/master segments. Further detail on this approach have been published elsewhere (Birke et al., 2013; Lipo et al., 2013).

2.3. Intravitreal injections

All animal studies were conducted in accordance with ARVO and European Union guidelines for the use of animals in ophthalmic and vision research. This study was approved by the Tufts University Institutional Animal Care and Use Committee. C57BL/6J (Jackson Laboratories) were maintained in accordance with federal, state and local regulations. Six-to ten-week old mice were anesthetized via an intraperitoneal injection of ketamine/xylazine mixture. Intravitreal injections were performed using a 32-gauge needle attached to a 5 μl syringe (Hamilton, Reno, NV) to deliver a 1 μl injection.

2.4. Laser induced choroidal neovascularization

Laser induced CNV was performed as described by us previously (Cashman et al., 2011). Briefly, mice were sedated with an intraperitoneal injection of ketamine (0.1 g/kg)/xylazine (0.01 g/kg) and pupils were dilated with one drop of 2.5% phenylephrine HCl (Bausch & Lomb Incorporate, Tampa, FL) and one drop of 1% Tropicamide (Bausch & Lomb Incorporate, Tampa, FL) per eye. To minimize corneal injury, one drop of 2.5% Hypromellolose (Goniovisc, Wellhead UK) was used and a coverslip attached. Four laser spots were created per eye at a spot size of 75 μm in diameter, 150 mW power and 100 ms pulse time using an argon laser (532 nm, IRIS Medical Light Solutions, IRIDEM, IRIDEX, Mountain View, CA).

2.5. Topical application of aptamers

1 nmole of AS1411 or CRO was diluted in 0.9% NaCl to a total volume of 20 μl. A total of 20 μl of the diluted AS1411, CRO or 0.9% NaCl (empty vehicle control) was administered per eye one day prior to laser treatment and every subsequent 24 h until the mice were sacrificed on day 7 post-laser injury.

2.6. GSL-I lectin, F4/80 and nucleolin staining

Mice were sacrificed by CO_2 inhalation, followed by cervical dislocation. Optic nerve, cornea, lens, iris and retina were removed and the posterior eyecups (RPE/sclera/choroid) were fixed overnight in 4% paraformaldehyde. Following fixation, eyecups were incubated at 37 °C in 2.5 mg/ml BSA in PBS for 30 min. Eyecups were then incubated at 37 °C in 100 mg/ml FITC-conjugated *Griffonia Simplicifolia* Lectin I (GSL-I, isolection B4, Vector Labs) in PBS for one hour. For nucleolin staining, eyecups were blocked in 6% normal goat serum for 30 min and then incubated with nucleolin antibody (NB600-241, Novus Biologicals, Littleton, CO) (1:50 dilution). Cy3 goat anti-rabbit (1:200) was used for 1 h at room temperature for secondary detection. Macrophage staining was performed using rat monoclonal anti-mouse F4/80 antibody (CI:A3-1; Abcam) followed by Cy3 goat anti-rat secondary antibody. Control staining of the posterior eyecup using both an isotype control primary antibody followed by secondary antibody, as well

as secondary antibody alone, were performed.

2.7. Measurement of laser spot size and statistics

For determining localization of FL-AS1411/FL-CRO following intravitreal injection, RPE/choroid/sclera (with retina removed) of treated eyecups were flatmounted and coverslipped. Images for each lesion were taken using an Olympus IX51 microscope with Retiga 2000R camera at the same exposure time. Images were exported to ImageJ (National Institutes of Health; Bethesda, MD, USA) for quantification of fluorescence intensity of image pixels. Background pixel intensity was determined for non-CNV lesion regions and subtracted from each image using ImageJ. For determining CNV area, images for each lesion were taken as described above and the area of staining was selected following subtraction of background pixel intensity using the freehand selection tool. Confocal images were captured using a Leica TCS SPE microscope (Leica Microsystems; Wetzlar, Germany). Statistical analysis was done for all assays using dual-tailed unpaired t-tests and performed using Prism 5 (GraphPad Software Inc, La Jolle, CA).

3. Results

3.1. AS1411 attenuates the formation of tubes by HUVECs in vitro

Prior to the formation of CNV, endothelial cells migrate from the choroid into the subretinal space and form neovascular membranes in response to elevated levels of cytokines such as VEGF (Grossniklaus et al., 2010). In order to determine whether AS1411 can inhibit endothelial cell migration and tube formation *in vitro*, we utilized the human umbilical vein endothelial cell (HUVEC) tube formation assay, a widely used model of *in vitro* angiogenesis. HUVEC cells were incubated with AS1411 or a negative control aptamer CRO at a concentration of 500 nM and the formation of master junctions, master segments and meshes was determined 20 h post incubation using the 'HUVEC angiogenesis analyzer' plugin for ImageJ. Media lacking CRO or AS1411 was used as an additional negative control. We determined a significant reduction in all three parameters for HUVECs incubated with AS1411 relative to CRO. Specifically, HUVECs incubated with AS1411 exhibited a 30.96% ± 6.78% ($p = 0.0038$); 24.26% ± 6.95% ($p = 0.013$) and 27.04% ± 9.36% ($p = 0.0277$) reduction in the number of master junctions, master segments and meshes respectively (Fig. 1A–D). We conclude that AS1411 attenuates the formation of tubes by HUVECs *in vitro*.

3.2. Cell surface nucleolin is expressed in laser-induced CNV

AS1411 has been found to bind nucleolin receptors on the cell membrane, and to be preferentially taken up by cells expressing high levels of surface nucleolin (Xu et al., 2001). While surface nucleolin expression has been reported on proliferating endothelial cells of tumor- or matrigel induced angiogenic vessels, expression on 'active' endothelial cells of the retina or choroid has not been previously reported (Huang et al., 2006). We investigated the expression of cell surface nucleolin on migrating endothelial cells post laser injury. Specifically, we utilized an argon laser to generate 4 laser burns in the Bruch's membrane of 6 week old C57BL/6J mice and harvested their eyecups four days post-laser injury and stained for endothelial cells using GSL-1 lectin or cell surface nucleolin using an anti-nucleolin antibody. As expected, GSL-I strongly stained the surface of cells at the center of the CNV lesion (Fig. 2A). Co-staining of eyecups with an antibody against nucleolin demonstrated co-localization of GSL-I and nucleolin. Confocal imaging and generation of serial images of the co-stained CNV lesions confirmed co-localization of the GSL-I and nucleolin staining (Fig. 2B). Additionally, confocal microscopy confirmed staining of cell surface nucleolin of the endothelial cells, and not nucleolin in either the cytoplasm or nucleus. We conclude that nucleolin is expressed on the surface of migrating endothelial cells in the laser-induced model of 'wet' AMD.

3.3. AS1411 localizes to the site of laser-induced CNV

In order to determine whether AS1411 may target cells within a CNV *in vivo*, 0.2 nmol of Alexa594 conjugated AS1411 (FL-AS1411) or a negative control aptamer (FL-CRO) was injected into the vitreous of mice at 4 days post-laser injury. Eyecups were harvested

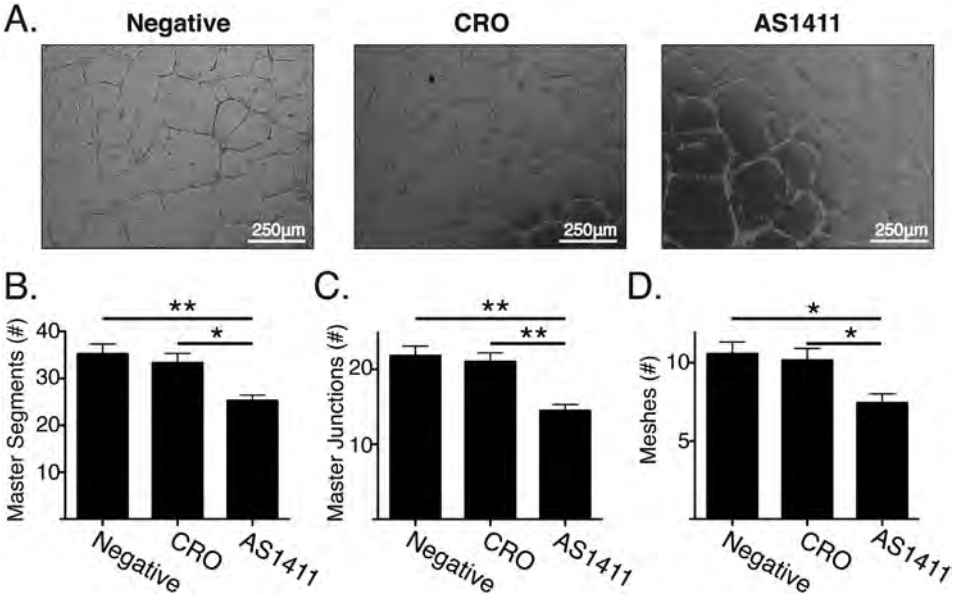

Fig. 1. AS1411 attenuates the formation of tubes by HUVECs *in vitro* A) Representative phase contrast images of tubes formed in the absence of supplements (negative control) or in the presence of 250 nM of CRO or 250 nM of AS1411. B–D) Quantification of mean number of master segments, master junctions and number of meshes formed in the presence of AS1411 or CRO. Studies were performed twice in duplicate and statistical significance was determined using two-tailed unpaired t-test.

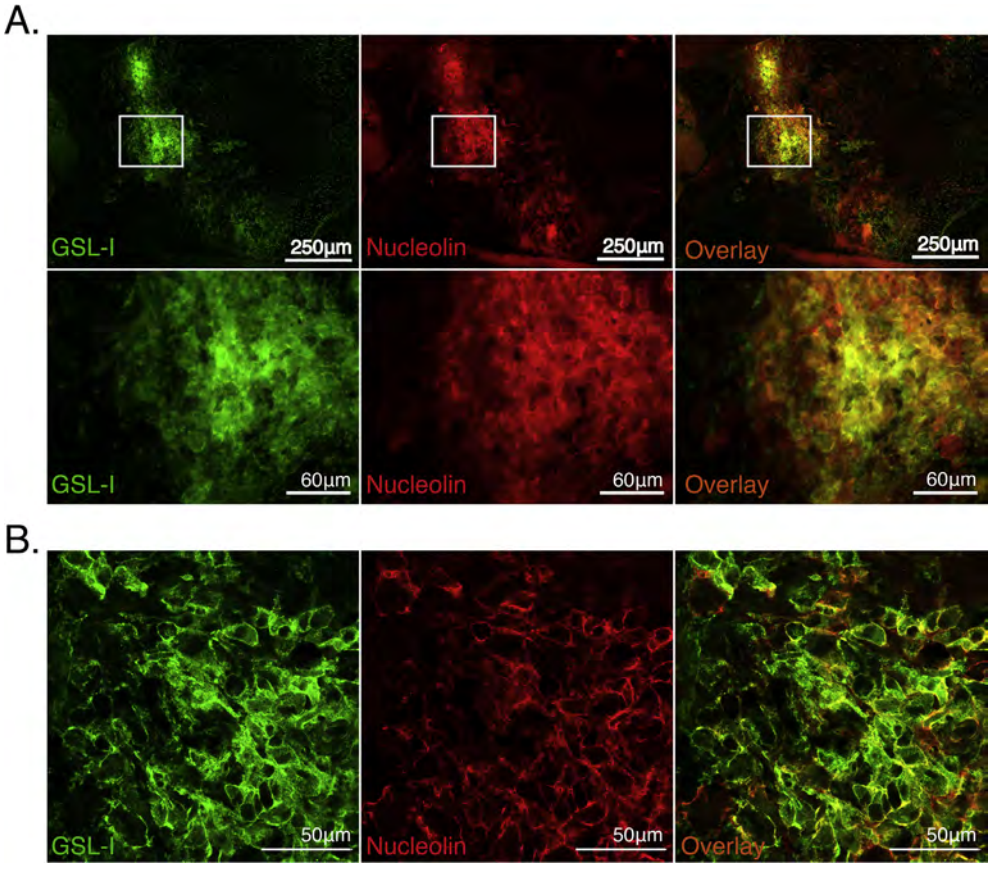

Fig. 2. Cell surface nucleolin is expressed in laser-induced CNV A) Representative images of murine eyecup harvested at 4 days post-laser captured with an inverted microscope. B) Representative confocal images of murine eyecup harvested at 4 days post-laser. Eyecups were stained for endothelial cell infiltration with GSL-I (green) and for surface nucleolin (red). Co-localization of GSL-I and nucleolin is shown in the overlay (yellow). N = 15 spots (5 eyes) (For interpretation of the references to color in this figure legend, the reader is referred to the web version of this article.).

2 h post-injection and stained for endothelial cells using FITC-labeled GSL-I. Analysis of Alexa594 fluorescence indicated a marked increase in fluorescence in the region of the GSL-I stained CNV lesion in those eyes injected with FL-AS1411 relative to those injected with FL-CRO (Fig. 3A). Quantification of the average Alexa594 fluorescence intensity in the CNV lesions of injected eyes demonstrated a 4.47 ± 0.69 fold increase ($p < 0.0001$) in intensity in FL-AS1411 injected mice relative to that of FL-CRO injected mice (Fig. 3B). We conclude that AS1411 localizes to migrating endothelial cells in the laser-induced model of CNV.

3.4. Intravitreal injection of AS1411 attenuates laser induced CNV

The aptamer AS1411 is known to bind to cell surface nucleolin, which in turn transports it to the nucleus and induces cell senescence (Xu et al., 2001). Since we found both increased expression of cell surface nucleolin as well as localization of intravitreally injected AS1411 to the site of laser-induced CNV, we hypothesized that AS1411 may be an effective inhibitor of CNV through inhibition of endothelial cell proliferation. To assess the potential of AS1411 as an anti-angiogenic agent, immediately following laser injury, mice were injected in the vitreous with 1 μl of PBS only, or PBS containing either 0.1 or 0.2 nmol of AS1411 or CRO. As a positive control for attenuation of laser-induced CNV, an additional set of mice were administered 2 pmol of a neutralizing antibody against mouse VEGF-A by intravitreal injection. This antibody has previously been shown to attenuate CNV formation when administered via subretinal or intravitreal injection (Nozaki et al., 2006; Liu et al., 2011). 7 days following laser injury, eyecups were harvested and stained for endothelial cell growth, using FITC-conjugated GSL-I. Although no significant attenuation of CNV growth was noted in eyes injected with the 0.1 nmol dose of AS1411, a significant reduction in CNV size was observed in those eyes injected with 0.2 nmol of AS1411 relative to eyes injected with either CRO or PBS (Fig. 4A). Specifically, measurement of the area of GSL-I positive staining indicated a 29.53 ± 12.58% reduction ($p = 0.0207$) and a 37.61 ± 12.63% reduction ($p = 0.0035$) in the size of CNV lesions in eyes injected with 0.2 nmol AS1411 relative to eyes injected with PBS or 0.2 nmol CRO respectively (Fig. 4B). Thus we conclude that 0.2 nmol is the minimally effective intravitreally injected dose of AS1411 required to attenuate formation of CNV. GSL-I staining indicated a 66.06 ± 12.56% reduction ($p < 0.0001$) in CNV size in eyes injected with the anti-VEGF antibody compared to those injected with PBS. Additionally, no significant difference in the size of CNV lesions was noted between 0.1 or 0.2 nmol CRO injected eyes relative to those injected with PBS. We conclude that intravitreal injection of AS1411 following laser injury attenuates choroidal neovascularization in the laser-induced model of 'wet' AMD and that this effect is not due to a non-specific response to oligonucleotides.

3.5. Intravitreal injection of AS1411 reduces infiltration of macrophages following laser induced CNV

Elevated levels of macrophages are present in the eyes of AMD patients as well as at the site of laser induced CNV (Penfold et al., 2001). Depletion of macrophages in the laser-induced model of

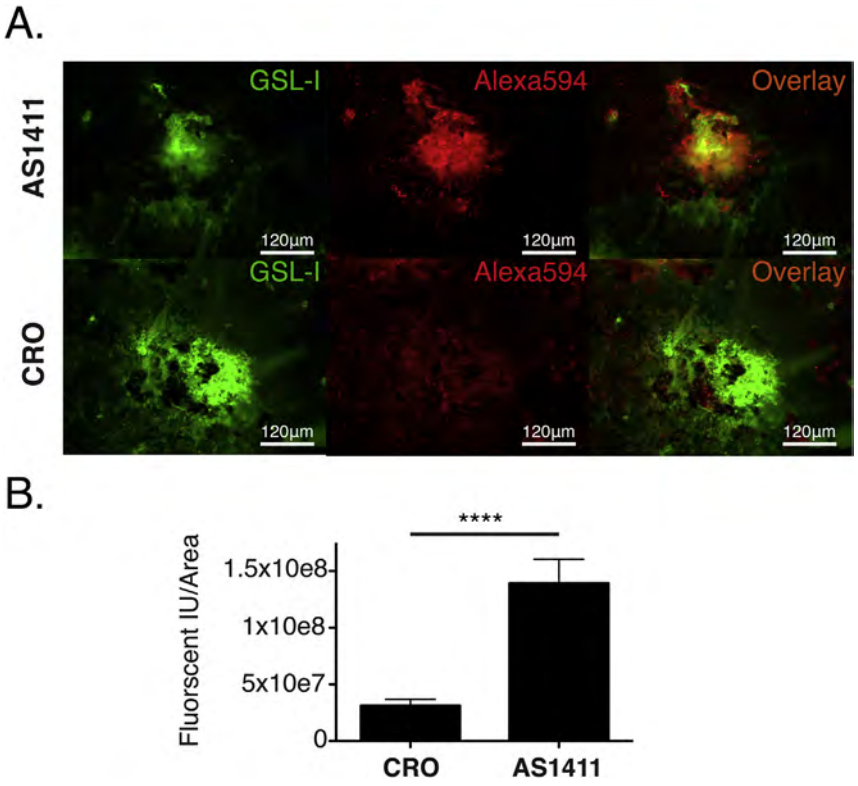

Fig. 3. AS1411 localizes to the site of laser-induced CNV A) Representative images of GSL-I stained CNV in a mouse eye intravitreally injected with 0.2 nmol of FL-AS1411 or FL-CRO at day 4 post laser and harvested two hours post injection. B) Quantification of fluorescent signal per CNV area for FL-CRO (32 spots/10 eyes) and FL-AS1411 (34 spots/10 eyes) injected eyes (****$p < 0.0001$)[two-tailed unpaired t-test].

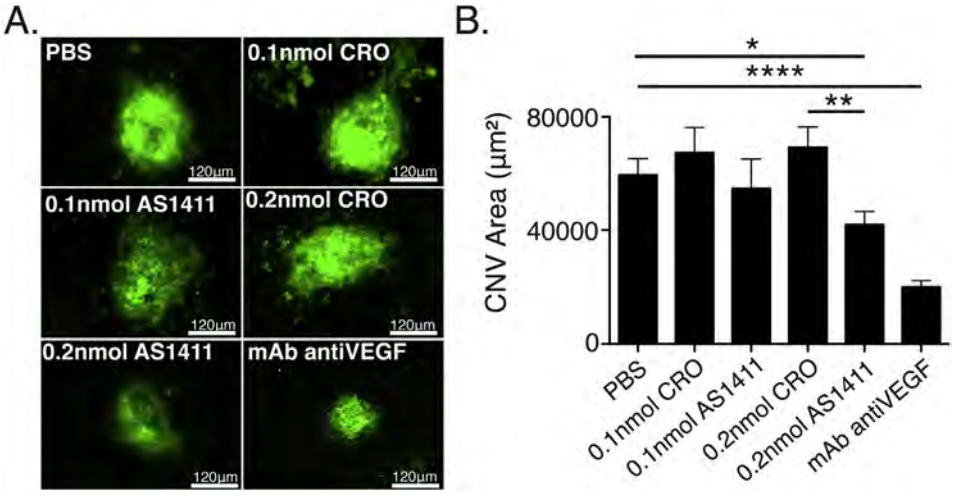

Fig. 4. Intravitreal Injection of AS1411 attenuates laser induced CNV A) Representative images of GSL-I stained CNV at day 7 post laser in a mouse eye intravitreally injected with PBS, 0.1 nmol of CRO, 0.1 nmol of AS1411, 0.2 nmol of CRO, 0.2 nmol of AS1411, or 2 pmol anti-VEGF antibody immediately following laser. B) Mean values ± SEM of CNV area of PBS injected eyes (44 laser spots/16 eyes); 0.1 nmol CRO injected eyes (28 laser spots/10 eyes); 0.1 nmol AS1411 injected eyes (36 laser spots/10 eyes); 0.2 nmol CRO injected eyes (60 laser spots/20 eyes); 0.2 nmol AS1411 injected eyes (65 laser spots/20 eyes), or anti-VEGF Ab injected eyes (29 laser spots/10 eyes); *$p = 0.0335$; **$p = 0.0035$; ****$p < 0.0001$ [two-tailed unpaired t-test].

'wet' AMD results in an attenuation of CNV (Penfold et al., 2001; Espinosa-Heidmann et al., 2003; Sakurai et al., 2003). Expression of cell surface nucleolin has been documented on monocytes and macrophages (Hirano et al., 2005). We hypothesized that AS1411 may impact the number of macrophages infiltrating the site of laser-induced injury in the model of wet AMD. Hence, we stained laser-induced CNV lesions of eyes injected with either AS1411 or CRO with an antibody against murine F4/80, a marker for macrophages (Fig. 5A). The average area of F4/80 staining observed in mice injected with AS1411 was 41,689 ± 6711 μm^2 relative to 69,840 ± 13459 μm^2 in mice injected with CRO, resulting in a 40.3% ± 19.8% ($p = 0.0485$) reduction in the area of macrophage infiltration (Fig. 5B). We conclude that AS1411 directly or indirectly inhibits macrophage infiltration in the murine laser-induced model of 'wet' AMD.

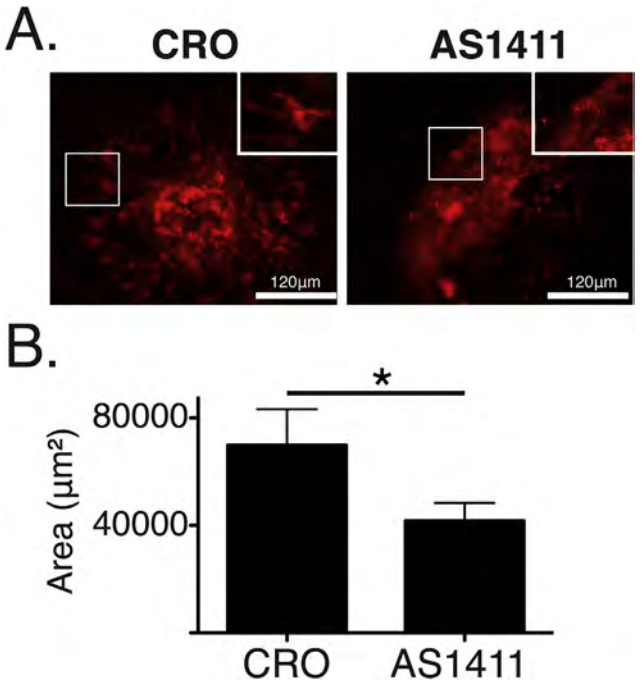

Fig. 5. Intravitreal injection of AS1411 reduces infiltration of macrophages following laser induced CNV A) Representative laser-induced CNV spots in murine eyecups stained with an antibody against the macrophage marker F4/80 in eyes intravitreally injected with 0.2 nmol CRO or 0.2 nmol AS1411. B) Quantification of the area of F4/80 staining indicated a significant reduction (40.3% ± 19.8%, $p = 0.0485$) in the area of macrophage staining in laser-induced CNV spots of eyes injected with 0.2 nmol of AS1411 (24 laser spots/6 eyes) relative to those injected with 0.2 nmol of CRO (17 laser spots/6 eyes) [two-tailed unpaired t-test].

3.6. Topical application of AS1411 attenuates laser induced CNV

The current standard of care for delivery of anti-VEGF molecules to the eye involves the use of an intravitreal injection (Keane and Sadda, 2012). As mentioned above, intravitreal injection is associated with a variety of complications, including patient discomfort and reduced compliance (Casten and Rovner, 2013). Hence, we wished to examine whether AS1411 may act as an inhibitor of CNV *in vivo* when delivered via topical application to the eye. We applied 1 nmol of AS1411 or CRO or normal saline buffer once daily for eight days topically to the eye, initiating one day prior to laser-induced injury. Posterior eyecups were harvested on day 7 post-laser injury and stained with GSL-I (Fig. 6A). The average size of CNV lesions was 14,909 ± 1995 μm^2 in eyes treated topically with AS1411, 26,325 ± 3494 μm^2 in eyes treated topically with CRO and 28,200 ± 2991 μm^2 in saline treated eyes (Fig. 6B). Topical treatment with AS1411, therefore, resulted in a 47.15% ± 12.58% ($p = 0.0003$) and 43.37% ± 15.57% ($p = 0.0066$) reduction in CNV size relative to saline treated or CRO treated eyes, respectively (Fig. 6B). CNV size between saline and CRO treated eyes was not significantly different ($p = 0.6893$). We conclude that topical application of AS1411 inhibits laser-induced CNV in a murine model of 'wet' AMD.

4. Discussion

This is the first study to examine the potential efficacy of a G-quartet aptamer targeting nucleolin in an animal model of 'wet' AMD. We report that expression of nucleolin is elevated on endothelial cells migrating in response to laser induced injury and that AS1411 co-localizes with nucleolin *in vivo* at the site of laser injury. Intravitreal delivery of AS1411 attenuates laser induced CNV and suppresses the infiltration of macrophages. Importantly, topical application of AS1411 also attenuates laser induced CNV. Our results have potential implications for the treatment of 'wet' AMD and possibly other ocular diseases involving choroidal neovascularization.

Due to the mounting evidence that VEGF plays a critical role in retinal homeostasis, one motivation for this study was to identify a therapeutic that did not directly target VEGF.

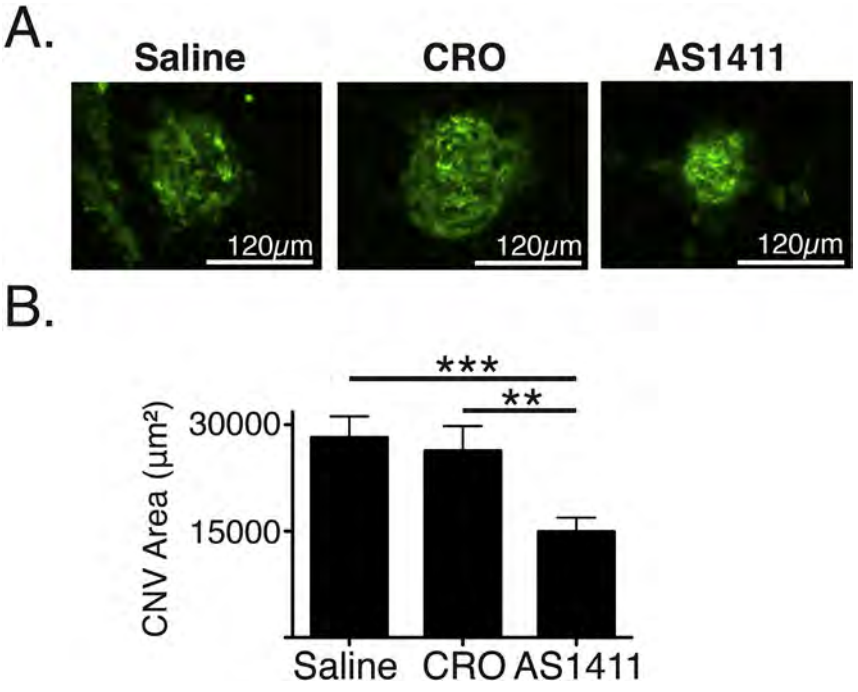

Fig. 6. Topical Application of AS1411 attenuates laser induced CNV A) Representative images of GSL-I stained CNV at day 7 post laser in a mouse eye topically treated one day prior to and 7 days post laser with 0.9% NaCl; 1 nmol CRO or 1 nmol AS1411. B) Mean values ± SEM of CNV area of eyes topically treated daily with 0.9% NaCl (39 laser spots/12 eyes); 1 nmol CRO (45 laser spots/13 eyes) or 1 nmol AS1411 (42 laser spots/12 eyes) (**$p = 0.0066$; ***$p = 0.0003$) [two-tailed unpaired t-test].

While anti-VEGF therapeutics can prevent loss of vision for a significant proportion of 'wet' AMD patients, recent evidence from clinical studies indicates that long-term inhibition of endogenous VEGF negatively influences the ocular architecture and exacerbates macular degeneration (Sacu et al., 2011; Campochiaro et al., 2014). Unlike ranibizumab or bevacizumab that act through VEGF, AS1411 acts through nucleolin. Cell surface nucleolin is not only present on mitotic cells; nucleolin has also been reported on the surface of bovine and C57BL/6J murine photoreceptors (Hollander et al., 1999; Conley and Naash, 2010). There is a potential, therefore, for binding and internalization of AS1411 by photoreceptors. However, as photoreceptors are post-mitotic and AS1411 acts by inducing cellular senescence through inhibition of DNA replication, the likelihood of AS1411 producing adverse off-target effects is reduced (Xu et al., 2001).

Comparison between current anti-VEGF treatments and intravitreal injection of AS1411 is not possible, since both *bevacizumab* and *ranibizumab* have been shown to be ineffective in the murine laser model of CNV (Lu and Adelman, 2009). Additionally, *pegaptanib sodium*, an aptamer targeting VEGF, did not exhibit any therapeutic effect in the murine laser induced model of CNV (Lu and Adelman, 2009; Lu and Adelman, 2009; Xu et al., 2001; Birke et al., 2013) Unlike these anti-VEGF therapies, AS1411 acts through nucleolin, which exhibits a high degree of evolutionary conservation, possibly allowing function of the aptamer across species. Due to the impracticality of testing equivalent concentrations of antibody to aptamer, the relative potency of the anti-VEGF antibody used in this study cannot be directly compared with the AS1411 aptamer, We can say, however, that our study indicates a more efficient minimum effective dose required for the anti-VEGF antibody than required for the nucleolin targeting AS1411. This could reflect the greater accessibility of a diffusible VEGF protein target by the intravitreally injected antibody than the surface bound nucleolin targeted by the AS1411 aptamer. This study warrants further investigation of nucleolin as a potential target for treating choroidal neovascularization.

Our studies were also motivated by the current limitations associated with administration of therapeutics for the treatment of 'wet' AMD via intravitreal injection every 4–12 weeks (Keane and Sadda, 2012). Each injection carries a risk for retinal detachment, hemorrhage and endophthalmitis (Sampat and Garg, 2010). Sustained elevation in intraocular pressure in normotensive eyes following intravitreal injections was noted to occur in patients treated with *bevacizumab* at <8 week intervals and intravitreal injections of *ranibizumab* and *bevacizumab* have been associated with ocular inflammation (Tolentino, 2011; Mathalone et al., 2012). Unlike some monoclonal antibodies associated with allergic infusion reactions, DNA aptamers, such as AS1411, are not significantly immunogenic, reducing the risk of such a reaction (Esposito et al., 2011). The significant burden placed on patients receiving injections every 4–12 weeks causes a reduction in quality of life and coupled with increased incidence of depression among this population can lead to decreased compliance (Goldstein et al., 2012). A therapeutic that could be administered noninvasively by the patient would overcome many of the issues associated with intraocular injections.

Due to the above unmet needs, the potential for inhibition of CNV through topically delivered drugs has been examined previously (Kiuchi et al., 2008; Sheu et al., 2009; Cloutier et al., 2012; Birke et al., 2013). In our studies, we found an approximate 45% reduction in CNV when 1 nmol (8.5 μg) of AS1411 was applied once daily one day prior and 7 days post-laser treatment. When 86 μg aganirsen, an antisense oligonucleotide that inhibits insulin receptor substrate (IRS)-1 expression, was topically applied two days prior and 14 days post-laser treatment, it was observed to result in almost complete inhibition of high grade laser induced CNV in African green monkeys (Cloutier et al., 2012). A nicotinic acetylcholine receptor antagonist, mecamylamine, was reported to reduce laser induced CNV by 35% when topically applied twice daily at 100 μg over the course of 7–14 days (Kiuchi et al., 2008). Topical application of 50 ng of vasostatin three times daily for 21 days was also shown to reduce laser induced CNV by approximately 50% in rats (Sheu et al., 2009). Additionally, we have recently found that topical application of 80 ng of PPADS, a P2X receptor antagonist, once daily for 3 days post laser treatment resulted in a 40% reduction in laser-induced CNV (Birke et al., 2013). We envisage that AS1411 may offer some unique advantages over other molecules in that it has already gone through clinical trials as a potential chemotherapeutic and was found to be well-tolerated in patients enrolled in a phase II trial in whom it was administered intravenously at 40 mg/kg/day over 1–4 days (Rosenberg et al., 2014). Another advantage of AS1411 is that DNA aptamers have a relatively low immunogenicity profile and synthesis of DNA aptamers is cost effective, reducing batch variability and potential viral or bacterial contamination associated with therapeutic antibody production (Esposito et al., 2011). While future studies examining the pharmacokinetic and toxicity profile of AS1411 will be required, in this study we have provided proof of concept that nucleolin is a target worthy of further investigation and that AS1411 has potential as a future treatment of AMD and possibly other ocular diseases involving choroidal neovascularization.

Acknowledgments

This study was supported by grants to R.K.S from The Paul and Phyllis Fireman Foundation, The Department of Defense/TATRC (W81XWH-12-1-0374), The National Institutes of Health/NEI (EY021805 and EY013837) and The Ellison Foundation.

References

Abdelmohsen, K., Gorospe, M., 2012. RNA-binding protein nucleolin in disease. RNA Biol. 9, 799–808.
Bates, P.J., Kahlon, J.B., Thomas, S.D., Trent, J.O., Miller, D.M., 1999. Antiproliferative activity of G-rich oligonucleotides correlates with protein binding. J. Biol. Chem. 274, 26369–26377.
Bates, P.J., Laber, D.A., Miller, D.M., Thomas, S.D., Trent, J.O., 2009. Discovery and development of the G-rich oligonucleotide AS1411 as a novel treatment for cancer. Exp. Mol. Pathol. 86, 151–164.
Bhutto, I., Lutty, G., 2012. Understanding age-related macular degeneration (AMD): relationships between the photoreceptor/retinal pigment epithelium/Bruch's membrane/choriocapillaris complex. Mol. Asp. Med. 33, 295–317.
Birke, K., Lipo, E., Birke, M.T., Kumar-Singh, R., 2013. Topical application of PPADS inhibits complement activation and choroidal neovascularization in a model of age-related macular degeneration. PLoS One 8, e76766.
Campochiaro, P.A., Wykoff, C.C., Shapiro, H., Rubio, R.G., Ehrlich, J.S., 2014. Neutralization of vascular endothelial growth factor slows progression of retinal nonperfusion in patients with diabetic macular edema. Ophthalmology 121, 1783–1789.
Cashman, S.M., Ramo, K., Kumar-Singh, R., 2011. A non membrane-targeted human soluble CD59 attenuates choroidal neovascularization in a model of age related macular degeneration. PLoS One 6, e19078.
Casten, R.J., Rovner, B.W., 2013. Update on depression and age-related macular degeneration. Curr. Opin. Ophthalmol. 24, 239–243.
Cloutier, F., Lawrence, M., Goody, R., Lamoureux, S., Al-Mahmood, S., Colin, S., Ferry, A., Conduzorgues, J.P., Hadri, A., Cursiefen, C., Udaondo, P., Viaud, E., Thorin, E., Chemtob, S., 2012. Antiangiogenic activity of aganirsen in nonhuman primate and rodent models of retinal neovascular disease after topical administration. Investig. Ophthalmol. Vis. Sci. 53, 1195–1203.
Conley, S.M., Naash, M.I., 2010. Nanoparticles for retinal gene therapy. Prog. Retin Eye Res. 29, 376–397.
Espinosa-Heidmann, D.G., Suner, I.J., Hernandez, E.P., Monroy, D., Csaky, K.G., Cousins, S.W., 2003. Macrophage depletion diminishes lesion size and severity in experimental choroidal neovascularization. Investig. Ophthalmol. Vis. Sci. 44, 3586–3592.
Esposito, C.L., Catuogno, S., de Franciscis, V., Cerchia, L., 2011. New insight into clinical development of nucleic acid aptamers. Discov. Med. 11, 487–496.
Ferrara, N., 2010. Vascular endothelial growth factor and age-related macular degeneration: from basic science to therapy. Nat. Med. 16, 1107–1111.

Funk, M., Karl, D., Georgopoulos, M., Benesch, T., Sacu, S., Polak, K., Zlabinger, G.J., Schmidt-Erfurth, U., 2009. Neovascular age-related macular degeneration: intraocular cytokines and growth factors and the influence of therapy with ranibizumab. Ophthalmology 116, 2393–2399.

Goldstein, J.E., Massof, R.W., Deremeik, J.T., Braudway, S., Jackson, M.L., Kehler, K.B., Primo, S.A., Sunness, J.S., 2012. Baseline traits of low vision patients served by private outpatient clinical centers in the United States. Arch. Ophthalmol. 130, 1028–1037.

Grossniklaus, H.E., Kang, S.J., Berglin, L., 2010. Animal models of choroidal and retinal neovascularization. Prog. Retin. Eye Res. 29, 500–519.

Heiduschka, P., Fietz, H., Hofmeister, S., Schultheiss, S., Mack, A.F., Peters, S., Ziemssen, F., Niggemann, B., Julien, S., Bartz-Schmidt, K.U., Schraermeyer, U., 2007. Penetration of bevacizumab through the retina after intravitreal injection in the monkey. Investig. Ophthalmol. Vis. Sci. 48, 2814–2823.

Hirano, K., Miki, Y., Hirai, Y., Sato, R., Itoh, T., Hayashi, A., Yamanaka, M., Eda, S., Beppu, M., 2005. A multifunctional shuttling protein nucleolin is a macrophage receptor for apoptotic cells. J. Biol. Chem. 280, 39284–39293.

Hollander, B.A., Liang, M.Y., Besharse, J.C., 1999. Linkage of a nucleolin-related protein and casein kinase II with the detergent-stable photoreceptor cytoskeleton. Cell Motil. Cytoskelet. 43, 114–127.

Hovanessian, A.G., 2006. Midkine, a cytokine that inhibits HIV infection by binding to the cell surface expressed nucleolin. Cell Res. 16, 174–181.

Hovanessian, A.G., Puvion-Dutilleul, F., Nisole, S., Svab, J., Perret, E., Deng, J.S., Krust, B., 2000. The cell-surface-expressed nucleolin is associated with the actin cytoskeleton. Exp. Cell Res. 261, 312–328.

Hovanessian, A.G., Soundaramourty, C., El Khoury, D., Nondier, I., Svab, J., Krust, B., 2010. Surface expressed nucleolin is constantly induced in tumor cells to mediate calcium-dependent ligand internalization. PLoS One 5, e15787.

Huang, Y., Shi, H., Zhou, H., Song, X., Yuan, S., Luo, Y., 2006. The angiogenic function of nucleolin is mediated by vascular endothelial growth factor and nonmuscle myosin. Blood 107, 3564–3571.

Keane, P.A., Sadda, S.R., 2012. Development of anti-VEGF therapies for intraocular use: a guide for clinicians. J. Ophthalmol. 2012, 483034.

Kiuchi, K., Matsuoka, M., Wu, J.C., Lima e Silva, R., Kengatharan, M., Verghese, M., Ueno, S., Yokoi, K., Khu, N.H., Cooke, J.P., Campochiaro, P.A., 2008. Mecamylamine suppresses Basal and nicotine-stimulated choroidal neovascularization. Investig. Ophthalmol. Vis. Sci. 49, 1705–1711.

Kurihara, T., Westenskow, P.D., Bravo, S., Aguilar, E., Friedlander, M., 2012. Targeted deletion of Vegfa in adult mice induces vision loss. J. Clin. Investig. 122, 4213–4217.

Lambert, V., Lecomte, J., Hansen, S., Blacher, S., Gonzalez, M.L., Struman, I., Sounni, N.E., Rozet, E., de Tullio, P., Foidart, J.M., Rakic, J.M., Noel, A., 2013. Laser-induced choroidal neovascularization model to study age-related macular degeneration in mice. Nat. Protoc. 8, 2197–2211.

Legrand, D., Vigie, K., Said, E.A., Elass, E., Masson, M., Slomianny, M.C., Carpentier, M., Briand, J.P., Mazurier, J., Hovanessian, A.G., 2004. Surface nucleolin participates in both the binding and endocytosis of lactoferrin in target cells. Eur. J. Biochem. 271, 303–317.

Lim, L.S., Mitchell, P., Seddon, J.M., Holz, F.G., Wong, T.Y., 2012. Age-related macular degeneration. Lancet 379, 1728–1738.

Lipo, E., Cashman, S.M., Kumar-Singh, R., 2013. Aurintricarboxylic acid inhibits complement activation, membrane attack complex, and choroidal neovascularization in a model of macular degeneration. Investig. Ophthalmol. Vis. Sci. 54, 7107–7114.

Liu, J., Jha, P., Lyzogubov, V.V., Tytarenko, R.G., Bora, N.S., Bora, P.S., 2011. Relationship between complement membrane attack complex, chemokine (C-C motif) ligand 2 (CCL2) and vascular endothelial growth factor in mouse model of laser-induced choroidal neovascularization. J. Biol. Chem. 286, 20991–21001.

Lu, F., Adelman, R.A., 2009. Are intravitreal bevacizumab and ranibizumab effective in a rat model of choroidal neovascularization? Graefes Arch. Clin. Exp. Ophthalmol. 247, 171–177.

Martin, D.F., Maguire, M.G., Ying, G.S., Grunwald, J.E., Fine, S.L., Jaffe, G.J., 2011. Ranibizumab and bevacizumab for neovascular age-related macular degeneration. N. Engl. J. Med. 364, 1897–1908.

Mathalone, N., Arodi-Golan, A., Sar, S., Wolfson, Y., Shalem, M., Lavi, I., Geyer, O., 2012. Sustained elevation of intraocular pressure after intravitreal injections of bevacizumab in eyes with neovascular age-related macular degeneration. Graefes Arch. Clin. Exp. Ophthalmol. 250, 1435–1440.

Nishijima, K., Ng, Y.S., Zhong, L., Bradley, J., Schubert, W., Jo, N., Akita, J., Samuelsson, S.J., Robinson, G.S., Adamis, A.P., Shima, D.T., 2007. Vascular endothelial growth factor-A is a survival factor for retinal neurons and a critical neuroprotectant during the adaptive response to ischemic injury. Am. J. Pathol. 171, 53–67.

Nozaki, M., Sakurai, E., Raisler, B.J., Baffi, J.Z., Witta, J., Ogura, Y., Brekken, R.A., Sage, E.H., Ambati, B.K., Ambati, J., 2006. Loss of SPARC-mediated VEGFR-1 suppression after injury reveals a novel antiangiogenic activity of VEGF-A. J. Clin. Investig. 116, 422–429.

Papadopoulou, D.N., Mendrinos, E., Mangioris, G., Donati, G., Pournaras, C.J., 2009. Intravitreal ranibizumab may induce retinal arteriolar vasoconstriction in patients with neovascular age-related macular degeneration. Ophthalmology 116, 1755–1761.

Penfold, P.L., Madigan, M.C., Gillies, M.C., Provis, J.M., 2001. Immunological and aetiological aspects of macular degeneration. Prog. Retin. Eye Res. 20, 385–414.

Rosenberg, J.E., Bambury, R.M., Van Allen, E.M., Drabkin, H.A., Lara, P.N.J., Harzstark, A.L., Wagle, N., Figlin, R.A., Smith, G.W., Garraway, L.A., Choueiri, T., Erlandsson, F., Laber, D.A., 2014. A phase II trial of AS1411 (a novel nucleolin-targeted DNA aptamer) in metastatic renal cell carcinoma. Investig. New Drugs 32, 178–187.

Sacu, S., Pemp, B., Weigert, G., Matt, G., Garhofer, G., Pruente, C., Schmetterer, L., Schmidt-Erfurth, U., 2011. Response of retinal vessels and retrobulbar hemodynamics to intravitreal anti-VEGF treatment in eyes with branch retinal vein occlusion. Investig. Ophthalmol. Vis. Sci. 52, 3046–3050.

Saint-Geniez, M., Kurihara, T., Sekiyama, E., Maldonado, A.E., D'Amore, P.A., 2009. An essential role for RPE-derived soluble VEGF in the maintenance of the choriocapillaris. Proc. Natl. Acad. Sci. U. S. A. 106, 18751–18756.

Saint-Geniez, M., Maharaj, A.S., Walshe, T.E., Tucker, B.A., Sekiyama, E., Kurihara, T., Darland, D.C., Young, M.J., D'Amore, P.A., 2008. Endogenous VEGF is required for visual function: evidence for a survival role on muller cells and photoreceptors. PLoS One 3, e3554.

Sakurai, E., Anand, A., Ambati, B.K., van Rooijen, N., Ambati, J., 2003. Macrophage depletion inhibits experimental choroidal neovascularization. Investig. Ophthalmol. Vis. Sci. 44, 3578–3585.

Sampat, K.M., Garg, S.J., 2010. Complications of intravitreal injections. Curr. Opin. Ophthalmol. 21, 178–183.

Sheu, S.J., Bee, Y.S., Ma, Y.L., Liu, G.S., Lin, H.C., Yeh, T.L., Liou, J.C., Tai, M.H., 2009. Inhibition of choroidal neovascularization by topical application of angiogenesis inhibitor vasostatin. Mol. Vis. 15, 1897–1905.

Tolentino, M., 2011. Systemic and ocular safety of intravitreal anti-VEGF therapies for ocular neovascular disease. Surv. Ophthalmol. 56, 95–113.

Ueta, T., Mori, H., Kunimatsu, A., Yamaguchi, T., Tamaki, Y., Yanagi, Y., 2011. Stroke and anti-VEGF therapy. Ophthalmology 118 (10), 2093–2093.e2.

Ueta, T., Yanagi, Y., Tamaki, Y., Yamaguchi, T., 2009. Cerebrovascular accidents in ranibizumab. Ophthalmology 116, 362.

Xu, X., Hamhouyia, F., Thomas, S.D., Burke, T.J., Girvan, A.C., McGregor, W.G., Trent, J.O., Miller, D.M., Bates, P.J., 2001. Inhibition of DNA replication and induction of S phase cell cycle arrest by G-rich oligonucleotides. J. Biol. Chem. 276, 43221–43230.